ABSTRACT

Partha Sarathi Nagchowdhuri. CONSEQUENCES OF REDUCED VERSICAN EXPRESSION IN EMBRYONIC CHICK SYNOVIAL JOINT DEVELOPMENT. (Under the supervision of Dr. Anthony A. Capehart). Department of Biology. April 2011.

The different mechanisms involved in vertebrate synovial joint development are actively being uncovered. A variety of studies have thus far discovered the involvement of several large molecules in the processes of joint development and cavitation. Such molecules include glycosaminoglycans, glycoproteins, proteoglycans, growth factors, and adhesive molecules. The coordinated spatiotemporal expressions of these molecules, among them chondroitin-sulfate proteoglycans (CSPG), are believed to play a crucial role in synovial joint formation. A previous study has shown that isoforms of the CSPG versican are abundantly expressed in the developing chick synovial joint during progressive stages of embryonic development (Shepard et al. 2007). The purpose of this study is to better understand the importance of versican in the developing limb joints by inhibiting its expression. We employed adenoviral-mediated RNA interference and *inovo* microinjection techniques to knock down endogenous versican protein levels. Results show an average reduction of 14% in the non-chondrogenic space of the joint interzone of day 10 embryos in response to versican knockdown that was coupled with attenuated expressions of key versican associating molecules such as hyaluronan, tenascin, CD44 and link protein. Impacts of versican knockdown also resulted in lowered collagen II expression among articular chondrocytes implying possible delays in chondrogenesis, or early transition toward an osteogenic fate.

Consequences of Reduced Versican Expression in Embryonic Chick Synovial Joint Development

A Thesis

Presented To

The Faculty of the Department of Biology

East Carolina University

In Partial Fulfillment

of the Requirements for the Degree

Master of Science in Biology

by

Partha Sarathi Nagchowdhuri

April 2012

CONSEQUENCES OF REDUCED VERSICAN EXPRESSION IN EMBRYONIC CHICK SYNOVIAL JOINT DEVELOPMENT

By

Partha Sarathi Nagchowdhuri

APPROVED BY:

DIRECTOR OF THESIS:_____
Anthony A. Capehart, Ph. D.

COMMITTEE MEMBER:_____
Paul Hager, Ph.D.

COMMITTEE MEMBER:_____
Laxmansa Katwa, Ph.D.

COMMITTEE MEMBER:_____
Charles A. Singhas, Ph.D.

COMMITTEE MEMBER:_____
Baohang Zhang, Ph.D.

CHAIR OF THE DEPARTMENT OF BIOLOGY:_____
Jeffery McKinnon, Ph.D.

DEAN OF THE GRADUATE SCHOOL:_____
Paul J. Gemperline, Ph.D.

Acknowledgements

First and foremost, I would like to thank Dr. Anthony Capehart for his immense patience and guidance throughout the duration of my Masters research project. There were times when I felt the project might lead to a dead end, but his encouragement and direction made it possible for me to better understand my project, ask pertinent questions, analyze options, and eventually find solutions. Overall, this project taught me a lot about how to ask questions as a scientist, analyze data, and make conclusions by piecing together results I obtained with those of others reported in the literature. Furthermore, I would like to thank him for challenging me to think critically, formulate hypotheses and predict possible outcomes—a skill paramount for being successful in research.

I also take the opportunity to thank the Department of Biology at ECU for the quality education I received as an undergraduate and graduate student. The faculty's constructive criticisms and encouragements have continued to fuel my interest in pursuing scientific research as a career.

Finally, I express my gratitude towards friends and family, who have prodded me with a stick throughout my Masters project, but expecially towards the end when it was time to submit my final thesis.

TABLE OF CONTENTS

LIST OF TABLES

LIST OF FIGURES

Consequences of Reduced Versican Expression in Embryonic Chick Synovial Joint Development

Development of the Vertebrate Limb and Synovial Joints

The tetrapod limb has served as an excellent model for studying differentiation and patterning in developing embryos. Previous studies have shown that the basic morphogenetic rules governing limb development are the same among all tetrapods. This was underscored by demonstrating that grafted pieces of mammalian or reptilian limbs were able to direct limb formation in chickens (Fallon and Crosby 1977; Sessions et al. 1989; Hinchliffe 1991). It was also shown that mesodermal cells are critical for limb development in all tetrapods by transplanting groups of limb mesodermal cells to different locations along the body axis resulting in limb formation at the corresponding areas (Hertwig 1925).

Limb Bud Initiation and Elongation

Vertebrate limb bud initiation commences with the allocation of specialized embryonic cells from the lateral plate mesoderm (LPM) into limb fields. The positioning and induction of limb fields along the embryonic axis have been characterized by differential *Hox* gene expression in the LPM: most importantly *Hox b6, Hox c8, and Hox b5* (Oliver et al. 1990; Rancourt et al. 1995; Nelson et al. 1996). A study involving mutant mice with disrupted *Hox b5* gene resulted in slightly displaced shoulder girdles along the embryonic axis (Rancourt et al. 1995). Specific combinations of several *Hox* gene expressions in the LPM and the embryonic trunk also determine the extent of limb outgrowth and the type of limb that develops (Cohn et al. 1997). Interestingly, it was shown that variations in *Hox* expression patterns in the LPM and the paraxial mesoderm are responsible for the absence of forelimbs in snakes (Cohn and Tickle 1999).

The initial limb bud consists of mesenchymal cells encased within an epithelial cell layer (Searls and Janners 1971). Along with *Hox* genes, limb induction also appears to be critically dependent on other factors. Retinoic Acid (RA), which possibly originates in Hensen's Node, appears to be crucial for initial limb bud differentiation as it facilitates regulation of *Hox* gene expression in the LPM during formation of limb fields (Hogan et al. 1992, Marshall et al. 1996). In a study where RA activity was blocked in the prospective limb areas in stage 12-18 chick embryos using the drug disulphiram, limb growth failed to occur (Stratford et al. 1996, Hamburger and Hamilton 1951). Growth Differentiation Factor 11 (GDF11) plays a vital role in limb positioning along the axial skeleton as mice deficient in the GDF11 gene developed hindlimbs that were displaced posteriorly along the body axis. This observation was coupled with an alteration of Hox gene expression patterns (McPherron et al. 1999) suggesting GDF11 and RA activity upstream of *Hox* genes in determining limb positioning and induction (Capdevilla and Belmonte 2001).

Following positional specification of limb fields along the embryonic flank, cells of the non-limb areas of the LPM divide at a much slower pace, whereas mesodermal cells of the LPM limb fields actively engage in cell proliferation, leading to a visible limb outgrowth or primordium (Searls and Janners 1971). In the chick embryo, limb buds are visible at stage 17, or embryonic day 3 (e3) (Hamburger and Hamilton, 1951). The cells of the LPM that give rise to the limb bud actively secrete fibroblast growth factor 10 (FGF10), which mediates signaling between the proliferating mesodermal cells and the overlying epithelial layer which is induced to form a thickened apical ectodermal ridge (AER). Mice deficient in FGF10 expression showed limb bud initiation, but no limb growth. Further analysis of the primordium showed no development of AER or zone of polarizing activity (ZPA) (Ohuchi et al. 1997, Sekine et al.

1999, Saunders 1948, Kieny 1960, Saunders and Reuss 1974). The cells of the AER in turn express FGF8, which keeps the underlying mesenchymal cells in a proliferative state allowing for limb outgrowth to occur through mitosis. This distal set of mesenchymal cells beneath the AER is referred to as the progress zone (PZ) as they allow limb elongation to occur (Mahmood et al. 1995, Crossley et al. 1996, Vogel et al. 1996, Ohuchi et al. 1997, Kawakami et al. 2001, Harrison 1918, Saunders 1948).

Classical experiments involving transplantations have shown that limb extension occurs along 3 axes: the proximal-distal (shoulder-digit) (PD), dorsal-ventral (knuckle-palm) (DV), and the anterior-posterior (thumb-fifth finger) (AP) axes (Johnson and Tabin 1997, Martin 1998). Each axis is associated with different organizing centers within the growing limb bud. The AER forming at the distal end of the limb bud facilitates continued limb extension along the PD axis (Tickle and Altabef 1999). John Saunders demonstrated that by removing the AER from the chick limb during early developmental stages total limb growth was severely compromised (Saunders 1948). Furthermore, it was shown that removing the AER at progressively later stages, more distal structures were able to form (Saunders 1948). The Zone of Polarizing Activity (ZPA) located at the posterior end regulates growth along the AP axis (Tickle et al. 1975). The protein sonic hedgehog (Shh), which is steadily expressed and secreted by the mesodermal cells of the ZPA, confers polarity to the posterior end (Riddle et al. 1993). The dorsal non-ridge ectoderm of the limb is the organizing center responsible for DV polarity, which is primarily mediated by Wnt-7a expression (MacCabe et al. 1974).

Chondrogenesis

In the developing vertebrate limb, skeletal structures form in a proximal-to-distal sequence. Mesenchymal cells that leave the progress zone early result in proximal structures

such as the stylopod (humerus or femur), whereas cells that leave the PZ at progressively later stages are destined to form more distal structures such as the zeugopod (radius and ulna or tibia and fibula) and eventually the autopod (carpus or tarsus and a variable number of digits) (Summerbell et al. 1973).

The chondrogenic process commences with the condensation of pre-cartilage mesenchymal cells of the growing limb bud that have exited the progress zone and therefore are out-of-reach of factors secreted by AER that keep cells in a proliferative state. These condensing mesenchymal cells aggregate into compact nodules that differentiate into chondrocytes (Hall and Miyake 1996). The induction and maintenance of these condensations are facilitated by expression and secretion of N-cadherin and N-CAM (Oberlender and Tuan 1994), as well as other factors, such as versican proteoglycan (Williams et al. 2005). In a study using the mouse chondrocytic cell line N1511, increased transcription and protein expression of chondroitin sulfate proteoglycan (CSPG) versican, especially V0 and V1 isoforms, was observed on treating the cells with chondrogenic stimuli such as parathyroid hormone and dexamethasone (Kamiya 2006). Versican is known to interact with other extracellular matrix (ECM) molecules such as type I collagen, fibronectin, hyaluronan, tenascin, and link protein via its chondroitin sulfate chains during mesenchymal condensation (Yamagata et al. 1986, Maleski and Knudson 1996, Matsumoto et al. 2003, Mackie et al. 1987, Aspberg et al. 1997). It was demonstrated *in vitro* that versican discourages mesenchymal cell adhesion to markers in the ECM like collagens and fibronectin suggesting versican's possible involvement in mesenchymal aggregation and chondrocyte differentiation (Yamagata et al. 1989). Not surprisingly, during the onset of mesenchymal condensation, fibronectin and type I collagen levels increase when compared to loose mesenchyme not undergoing condensation. On chondrocyte maturation, however, type I

collagen gets gradually replaced by type II collagen, while fibronectin levels begin to disappear (Dessau et al. 1980). The mesenchymal condensation process initially gives rise to the cartilage anlage, which further undergoes skeletogenesis through the endochondral pathway (Fell 1925, Thorogood and Hinchliffe 1975, Jurand 1965).

Formation of Synovial Joints

Synovial joint formation along the embryonic limb begins with the flattening and packing of non-chondrogenic mesenchymal cells to form the joint interzone (Archer et al. 2003, Craig et al. 1987). Even though pathways that dictate synovial joint positioning along the embryonic limb are not fully understood, it has been suggested that joint locations are prespecified within the mesenchymal condensations of the early limb bud (Khan et al. 2007, Holder 1977, Pacifici et al. 2005). Joint interzones in the developing embryo are comprised of a central intermediate zone that is sandwiched between two chondrogenous layers lining the epiphyseal ends of the long bone anlagen (Craig et al. 1987, Ito and Kida 2000). It is believed by some that the articular cartilage is derived from the cells of the intermediate zone as the outer layers differentiate into chondrocytes and add to the growing anlagen (Archer et al. 1994, Ito and Kida 2000). It was also reported that unlike the mesenchymal cells involved in the formation of long bone cartilage, joint interzone cells are interconnected by gap junctions, implying close cooperation between interzonal cells and synchronized operation in forming the joints (Archer et al. 2003, Pacifici et al. 2005).

Synovial joint formation hinges critically on the activity of certain key growth factors, transcription factors, and signaling molecules. Growth differentiation factor-5 (GDF-5) is one of several key molecules needed for synovial joint initiation since its expression is detected in the early chick and mouse joint interzones and even throughout the early mesenchymal

condensations (Storm and Kingsley 1996). Mutant mice lacking the GDF-5 gene showed joint deformities such as brachypodism and defects in overall skeletal growth (Storm et al. 1994, Settle et al. 2003). In addition to GDF-5, other factors such as Wnt-14, β-catenin, and proteoglycans also appear to play decisive roles in establishing the joint interzone. The Wnt-14 isoform is expressed in the presumptive joint, and its overexpression in chick embryo limbs drives the ectopic expression of other interzone markers such as GDF-5, Chordin and CD44 (Hartmann and Tabin 2001). Not surprisingly, it was observed that conditional ablation of the Wnt signaling mediator β-catenin in mouse embryo limb chondrocytes resulted in absence of synovial joints (Guo et al. 2004). These and other findings have led a number of research groups to propose that Wnt-14 solely is sufficient for proper synovial joint formation as it acts as an upstream regulator of key joint markers such as GDF-5 and β-catenin, and maintains the mesenchymal nature of the interzone cells by preventing further differentiation into chondrocytes (Hartmann and Tabin 2001, Guo et al. 2004).

The smooth functioning of synovial joints during later stages of life strongly hinges on the process of embryonic synovial joint cavitation, or the timed partitioning of the interzone tissue that connects the two opposing joint-forming skeletal structures together (Pacifici et al. 2005). Several preliminary studies argued mechanical movement as the cause of joint cavitation, whereas others implicated mechanical movement in maintaining the joint cavity (Murray and Selby 1930, Hamburger and Waugh 1940, Fell and Canti 1934). Recent studies however have indicated that cavitation is primarily a result of increased expression of Hyaluronic acid (HA) and its cell surface receptor CD44 in the interzone (Craig et al. 1990, Archer et al. 1994, Edwards et al. 1994, Pitsillides et al. 1995). Moreover, the inhibition of HA in the interzone,

whose accumulation is believed to discourage tissue integrity, led to the inhibition of cavitation (Dowthwaite et al. 1998).

A vital component of synovial joints is the articular cartilage that forms the "boundaries" of synovial joints. Articular chondrocytes differ from the transient chondrocytes forming the long bone anlagen in that the former retain their phenotype throughout the life of the organism, tend to be less mitotic, and pack more densely during embryonic joint development (Lufti 1974, Howlett, 1979). Articular cartilage persistently imparts functional resilience to the joints and resists ossification unlike skeletal cartilage tissue, which undergoes cellular hypertrophy, apoptosis and inevitable replacement by osteoblasts (Pacifici et al. 2005, Jurand 1965). Furthermore, spatial and temporal expression of markers such as collagens, tenascins, and chondroitin sulfate proteoglycans (CSPGs) confer to it tensile strength and elasticity (Hay 1991).

CSPGs and Versican

Proteoglycans, or core proteins covalently linked to glycosaminoglycan (GAG) side chains, are highly expressed in developing cartilage and synovial joint matrix. They interact with various molecules in forming and maintaining the joints and cartilage via their GAG side chains or terminal domains. Proteoglycans are especially versatile in forming complexes with ECM components, keeping cells attached to the ECM, and maintaining tissue structure and integrity (reviewed in Rouslahti 1989). Chondroitin sulfate proteoglycans (CSPGs) or proteoglycans with chondroitin sulfate (CS) GAG chains such as versican play critical roles in the skeletal development of limbs and joints, and is the subject of this study. CSPG Versican has been found to be highly expressed in the ECM during chondrogenesis and its spatial and temporal distribution pattern is believed to be crucial in limb and synovial joint formation (Shepard et al. 2007).

Alternate splicing of versican (*cspg*-2 gene) mRNA leads to the generation of four isoforms, all of which consists of globular N-terminal G1 and C-terminal G3 domains (Zimmermann and Rouslahti 1989). The N-terminal G1 domain of versican consists of immunoglobulin (IgG)-like motifs followed by two-link protein like motifs. It interacts with hyaluronic acid specifically, and this complex is further stabilized by association with link protein (LP), which facilitates a loose and highly hydrated extracellular environment (Le Baron et al. 1992, Lee et al. 1993, Wight 2002, Yamagata et al. 1993). The C-terminal G3 domain interacts with molecules such as fibrilin-1 and tenascin, and consists of a C-type lectin-like domain, two epidermal growth factor like repeats, and a complement regulatory domain (Isogai et al. 2002, Aspberg et al. 1997, Olin et al. 2001, Shinomura et al. 1993).

The unspliced versican isoform (Vo), with a molecular weight of more than one million Daltons consists of two chondroitin sulfate (CS α and CS β) attachment sites between the G1 and G3 domains (Shinomura et al., 1993). The other spliced forms of versican are V1, V2 and V3 isoforms. The V1 isoform consists of G1, CSß, and G3 domains; whereas the V2 isoform consists of G1, CSα, and G3 domains. The V3 isoform contains only the G1 and G3 domains (Kamiya et al. 2006).

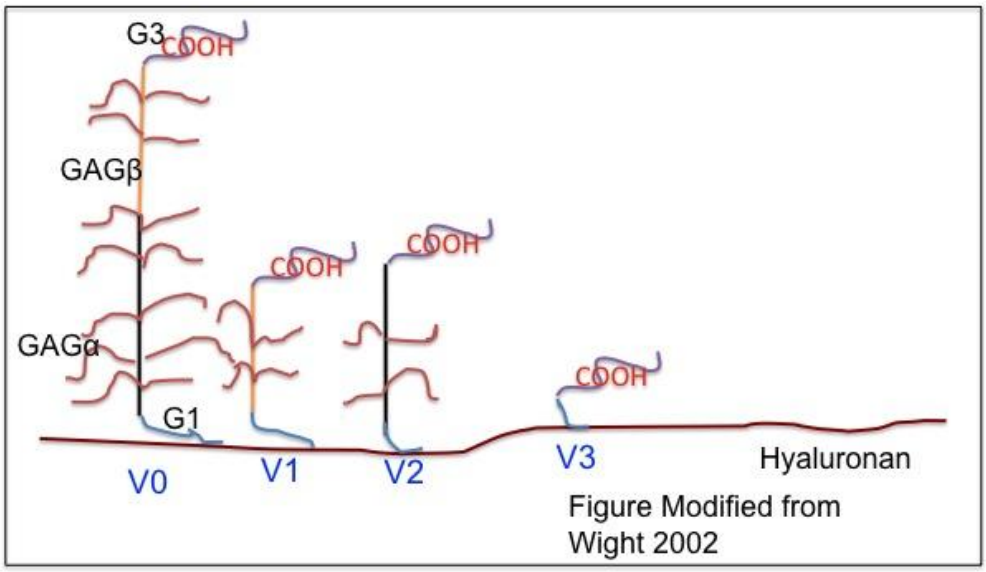

Versican in Synovial Joint development

A previous study conducted by our laboratory showed varied versican expression during progressive stages of chick limb development. Initially, there was uniform versican expression in the whole limb primordium. However, at progressively later stages, versican was more defined in the synovial joints, whereas other markers such as aggrecan and collagen II were restricted to mature chondrocytes of the skeletal template (Shepard et al 2007). Another study utilizing morpholinos to silence versican expression in the developing chick limb between HH stages 22 and 37 (e3.5-11) resulted in reduced zeugopod and autopod phenotypes (Shepard et al. 2007). This study attempts to extend our understanding of versican's function in synovial joint and articular cartilage morphogenesis by using adenovirally encoded shRNAs to assess impacts of versican knockdown during synovial joint development.

Materials and Methods

ShRNA Adenovirus Preparation

shRNA Design and Cloning

Our lab designed five short hairpin RNA (shRNA) templates that target versican mRNA at nucleotide positions 36, 320, 768, 10330, and 10456 along with a scrambled negative control that is non-specific for any RNA sequence. A published shRNA sequence targeting versican mRNA at position 5334 was also used (Sheng 2006). The NCBI BLAST (Basic Local Alignment Search Tool) tool was used to verify that the shRNA sequences did not match any of the other RNA sequences in the chick genome. The p*Silencer* adeno 1.0-CMV system (Ambion Catalog# 5790) was used to construct shRNA adenoviral constructs. The shRNA templates were first ligated into the p*Silencer* shuttle vector containing a CMV promoter using DNA ligase. The ligation reactions were then used to transform JM109 (Promega) competent *E. coli* cells. Plasmids containing the shRNA sequences were isolated using QIAprep Spin Miniprep kit (Qiagen). The Shuttle Vector clone plasmids were then sequenced using the forward sequencing primers provided in the P*Silencer* kit to verify correct shRNA sequence. Following sequencing, the shRNA plasmids were amplified in large-scale *E. coli* cultures to obtain a minimum plasmid concentration of at least 500ng/μl for adenoviral preparation.

Preparation of Recombinant Adenovirus using p*Silencer* Adeno 1.0 CMV system

For preparation of each recombinant shRNA adenovirus, the corresponding plasmid and *Lac Z* adenoviral backbone from the p*Silencer* kit was linearized using *Pac*1 restriction endonuclease according to kit instructions. Calcium phosphate transfection media (Clontech) was used to co-transfect the linearized digestion products into low density HEK 293 cells in DMEM (Dulbecco Modified Eagle's Media) cell culture media containing 10% heat inactivated

fetal bovine serum (FBS) and 1% penicillin/streptomycin (Gibco). DNA recombination was allowed to occur for about two weeks or until cytopathic effect (CPE) was confirmed. This was usually detected by the presence of adenoviral foci evidenced by detached cells. At approximately 50% CPE, cells were mechanically detached, lysed using three consecutive freeze-thaw cycles, and the supernatant was collected via centrifugation. The supernatant, which is expected to contain packaged adenoviruses, was used to infect low density HEK-293 cells in 60 mm cell culture plates for initial expansion of the recombinant adenoviruses. After adequate cytopathic activity was observed (at least 60% of the cells were detached), the cells were removed from the plate and transferred to a 10 mL conical tube. The cells were lysed, centrifuged, and the supernatant was used to infect low-density cells in 75cm^2 cell culture flasks for further expansion of the adenoviruses. The same lysis procedures were repeated to harvest adenoviruses from the large-scale cultures.

Adenovirus Purification and Titration

Following cell lysis and adenovirus harvest, the viruses were purified using the Adeno-X Virus Mini Purification Kit (Clontech) according to kit instructions. A total of 0.4 mL of adenovirus was eluted form each preparation, and 80 μL of cryopreservative was added to each eluate.

The adenoviruses were then diluted to concentrations of 10^{-4}, 10^{-5}, and 10^{-6} in DMEM, and used to infect HEK-293 cells at 60% confluency for 48 hours in a 37^{o}C cell culture incubator with humidified 95% air, 5% CO_2. Following incubation, the cells were fixed with ice-cold 4% paraformaldehyde in phosphate buffered saline (PBS) for 10 minutes at room temperature, and subsequently washed three times with PBS. The cells were then incubated in X-gal staining solution (0.02% magnesium chloride, 0.1% potassium ferrocyanide, 0.1% potassium

ferricyanide, 0.1% Xgal in PBS) until blue Lac Z postive cells were visible. An inverted microscope with a 20X objective lens was used to count the number of lacZ positive cells in twelve random fields. The average number of Lac Z cells per field was used to calculate the adenoviral titer (in infectious units (IFU) / mL) using instructions provided in the Adeno-X Rapid Titer Kit User Manual (Clontech). Adenoviral aliquots were kept at -70^{o}C freezer for long-term storage.

Assessment of versican knockdown using Chick Embryo Fibroblasts and Real-time PCR

Chick Embryo Fibroblast Cell Cultures

Chick embryo fibroblast (CEF) cells were isolated from dermal tissues of a day 10 chick embryo in PBS. The tissues were digested with 0.25% Trypsin/EDTA (Invitrogen) for 10 minutes at 37^{o}C. Following digestion, an equal volume of 1:1 DMEM/F12 media containing 10% FBS was added to the digested cells to quench Trypsin activity. The cells were centrifuged at 1000rpm for 5 minutes, and the media was replaced with fresh culture media containing 2% FBS. The cell density was evaluated using a hematocytometer, and adjusted to 250,000 cells per 50 µl volume.

Adenoviral Infection and RNA Extraction

Three biological replicate cell cultures, each consisting of 2 million cells, were used for each adenovirus being tested. The cells were either infected with the 320-virus (viral titer, 5 x 10^{9} ifu/mL), 5334-virus (viral titer, 5 x 10^{9}ifu/mL) or left untreated as a negative control. The 320-adenovirus was chosen since it showed the best versican silencing activity in *in-vitro* micromass cultures. In the viral treated cultures, a MOI (multiplicity of infection) of 100 was used when infecting the cells. After infection, the cells were seeded in 35 mm culture plates and each plate was flooded with 2 mL of DMEM/F12 media containing 2% FBS and incubated. The

culture media was replaced after 24 hours with fresh media containing 10% FBS. Total RNA was extracted from all the replicates following 48 hours of infection using the RNA aqueous-4 PCR kit (Ambion). RNA concentrations were measured using an Eppendorf *Biophotometer*.

Real Time PCR

The Superscript III First Strand Synthesis kit (Invitrogen) was used to reverse transcribe 350ng of total RNA from each biological replicate. Oligo dT priming was used so that only mRNA would be reverse transcribed. The synthesized cDNA-mRNA hybrid was further treated with RNase H to degrade complementary mRNA strands. The cDNA from each replicate was then diluted three-fold in nuclease free water and used for real time PCR. Two sets of primers were designed for the PCR reactions: one flanking position 320 (for the 320-virus treated cells F: AACGTCAGTCCTTCCATGCT, R: TGAATGGGTTGGAACAGACA), and another flanking position 5334 (for the 5334-virus treatment F: CCTTTTGAAAGCAACCCAGA, R: TGTGCCAGAAGCCAAAGAAG). The real-time PCR reactions were performed in an Applied Biosystems ABI 7300 Real-time PCR machine using RT^2 Real-Time ^{TM} SYBR Green /Rox PCR master mix (SuperArray) according to manufacturer's instructions. ß-actin primers (F: CACAGATCATGTTTGAGACCTT, R: CATCACAATACCAGTGGTACG) were used to amplify endogenous ß- actin as an internal control (De Boever et al. 2008). Threshold cycle data was analyzed using MS Excel and the Paffle method was used for relative quantification calculations (Pfaffl 2001). Student-t test was also performed to evaluate statistical significance.

In-ovo Microinjections

Fertilized, viral-free chick eggs (Charles River) were incubated in a 37.5^{o}C humidified egg incubator until the embryos developed to day 5 (e5) or Hamburger and Hamilton (HH) stages 24.5-25. The eggs were 'windowed' and the eggshell and vitellin membranes were

carefully removed using tungsten needles. The presumptive elbows of the accessible wings (usually the right wing) were injected with 1.5µL of either the control shRNA virus, 320-virus, 5334-virus, or a 1:1 combination of the 320 and 5334 viruses (0.75µL + 0.75 µL). The uninjected wings served as contra-lateral controls (CLC). The viruses were transported into the wings using pulled-glass needles inserted into a Narashige Micromanipulator connected to a pneumatic pump (Model 820, WPI). Each microinjection delivered approximately 7.5 x 10^6 virions. Furthermore, to verify that the viral media itself was not influencing the resulting phenotype, vehicle injection controls were also performed. The windowed eggs were sealed with clear plastic tape and the eggs were placed back in the incubator until desired developmental stages were reached (usually HH stages 33-34 or HH stage 36; e8 or e10). The embryos were then harvested, and preserved using appropriate fixatives.

Whole Mount ß-galactosidase reactivity

The ß-galactosidase staining procedure was adapted from (Kern et al. 2007). Virally injected embryos were first fixed in ice cold PBS containing 4% paraformaldehyde for 40 minutes. The fixation was stopped by removing the paraformaldehyde and rinsing the embryos three times with PBS for 5 minutes each rinse. The embryos were then washed in a detergent based permeablilizing buffer (.02% sodium deoxycolate, .01% Tergitol–type NP-40 in PBS) three times, five minutes each wash, and rocked overnight at 4^{o}C in the permeablizing buffer. Following extensive permeablization, the embryos were incubated in a ß-galactosidase staining buffer containing 0.02% magnesium chloride, 0.1% potassium ferrocyanide, 0.1% potassium ferricyanide, and 0.1% X-gal (Invitrogen) or Red Gal (Research Organics) in PBS at 37^{o}C in the dark until a characteristic blue or red color was apparent at sites of viral infection. Specimens were fixed once more with 4% paraformaldehyde for 15-20 minutes to quench further ß-

galactosidase reactivity, and washed three times with PBS. For further storage, the embryos were kept in PBS at 4^{o}C or embedded in paraffin.

Whole Mount Alcian Blue/ Alizarin Red Histochemistry

Histochemical staining procedures were employed to analyze *in-vivo* effects of versican knockdown in the synovial joints of whole mount specimens. Alcian blue/Alizarin red whole-mount histochemistry was used to detect gross morphological changes in the elbow phenotype. The impacts on various molecular markers were detected using immunohistochemistry. Day 10 embryos were fixed in 95% ethanol overnight at room temperature, followed by overnight staining in 0.2 % alcian blue in acidified ethanol (pH 1). The embryos were rinsed twice with 95% ethanol for 1 hour each for removal of excess alcian blue stain. Following the ethanol washes, the embryos were macerated with 2% potassium hydroxide (KOH) until the embryos were translucent (usually 3-5 hours; Kuczuk and Scott 1984). The embryos were then stained with 0.01% Alizarin Red and further cleared using serial KOH/glycerol washes (80:20, 60:40, 40:60, 20:80) approximately 60 minutes each wash. The embryos were kept in 100% glycerol for long-term storage (Kuczuk and Scott, 1984).

Immunohistochemistry

Paraffin sections (7 µm) or cryostat sections (10µm) wide were stained with the following primary antibodies: rabbit anti-chick versican (1:50; Zanin et al. 1999), rabbit anti-phosphohistone H3 (1:100, Cell Signaling), monoclonal mouse supernatants anti-collagen II, mouse anti-chick tenascin, mouse anti-chick CD44, and mouse anti-link protein (Developmental Studies Hybridoma Bank, Iowa City, IA) (1:5 dilutions). Biotinylated hyaluronic acid binding protein (HABP) (1:100, Cape Cod) was used to localize extracellular hyaluronic acid. Secondary immunoreagents used were FITC-conjugated Strepavidin, fluorescein or rhodamine

conjugated goat anti-mouse or –rabbit antibodies (ICN-Cappel). HABP and strepavidin were diluted 1:100 in PBS, whereas all other primary and secondary antibodies ere diluted in PBS containing 3%BSA (Bovine Serum Albumin) and 1% NGS (Normal Goat Serum). Before primary antibody incubation, sections were treated with Citrate-based Antigen Unmasking solution (Vector Labs) and 1mg/mL Bovine testicular hyaluronidase (Sigma), except for sections reserved for HABP or CD44 staining which were treated with .25U/mL Chondroitin ABC lyase (Sigma). Following staining, the sections were post-fixed in 80% and 50% ethanol, and reequilibrated in PBS. Sections were mounted with coverslips using 10% PBS-90% glycerol containing 100 mg/mL 1,4-diazabicyclo (2,2,2) octane (DABCO) (Sigma) and viewed using an Olympus BX-40 microscope equipped with epifluorescence optics. Images were captured using a SPOT-RT camera and software (diagnostic Instruments).

TUNEL Assay

The TUNEL (Terminal deoxynucleotidyl transferase dUTP nick end labeling) assay using the ApopTag Peroxidase *In Situ* Apoptosis Detection Kit (Chemicon) was used to assay apoptotic cells by detecting DNA fragmentation characteristic of programmed cell death. In this procedure, slides containing paraffin sections were first deparaffinized and equilibrated in PBS. Sections were then incubated in 20 µg/mL Proteinase K in PBS for 15 minutes at room temperature, washed three times with PBS to stop enzyme action, and further incubated in 3% hydrogen peroxide in PBS for 5 minutes to quench endogenous peroxidase activity. Thirty-µL of kit supplied equilibration buffer was added to each specimen and incubation was allowed for 10 seconds at room temperature. The equilibration buffer was then aspirated and 30 µL of working strength TdT (Terminal deoxynucleotidyl Transferase) enzyme was immediately added to each specimen and incubated at 37^{o}C in a humidified chamber for 1 hour. The TdT enzyme reaction

was inhibited using a working strength Stop/Wash Buffer provided with the kit. Following three serial PBS washes, the specimens were incubated in Anti-Digoxigenin conjugate for 30 minutes at room temperature. The specimens were washed with PBS three times and incubated in a developing solution containing hydrogen peroxide and 3,3' Diaminobenzidine (DAB) until characteristic brown cells were visible. Sections were mounted with Permount and viewed using light microscopy.

Results

To better understand versican function in synovial joint development and morphogenesis, we employed an adenovirally mediated RNA-interference strategy utilizing short hairpin RNAs or shRNAs. ShRNAs facilitate site directed cleavage and degradation of mRNA transcripts by activating endogenous RNA-Induced Silencing (RISC) complexes. Quantitative real-time PCR assessment of shRNA activity of the adenoviruses on chick embryo fibroblasts (CEF) cell cultures resulted in 70% knockdown in versican mRNA levels on treatment with the 320-shRNA virus, and 50% knockdown when treated with the 5334-shRNA virus following 48 hours of infection when compared to an untreated negative control group (Fig.1). The *Student t* test was performed to ensure that the knockdowns were statistically significant. The following null hypothesis was tested: There is no difference in the levels of versican mRNA among the untreated and adenovirally treated groups of CEF cells. Statistical significance was set at $p<0.05$. Both experimental groups showed statistically significant knockdown in the levels of versican mRNA. Furthermore, combined *in ovo* injections of the 320 and 5334-shRNA adenoviruses into chick elbows led to an average reduction of 65% in versican mRNA levels five days following injection when compared with the control adenovirus (Fig. 2). Versican protein knockdown was assessed by immunostaining with polyclonal rabbit-anti chick versican antibodies (Zanin et al. 1999). Reductions in versican staining in synovial joint interzones and articular chondrocytes was visible on paraffin sections of wrists injected independently with 320-shRNA (Fig. 3), or elbows injected with 5334-shRNA (Fig. 7 D,E) or combined (320+5334) shRNA viruses (Fig.6 G,H). No versican silencing, however, was noticeable for the control shRNA adenovirus (Fig. 5 C,D). Figure 3B shows versican protein knockdown in a HH stage 36 (e10) wrist (carpal) joint previously injected with 320-shRNA adenovirus. On comparison with the contralateral control

(CLC) wrist joint (Fig. 3A), a clear reduction in versican expression is apparent in the distal articular surface of the ulna and the central lamina of the carpal interzone in the injected wing. Sites of shRNA transfection were detected from the blue staining resulting from the reaction between β-galactosidase reporter and X-gal.

Overall effects on synovial joint morphology of shRNA transfection into HH stage 25 chick elbows were evaluated at HH stages 36-37 (e10) using Alcian Blue and Alizarin Red histochemistry. We noticed an overall 14% average decrease in joint spacing (the clear space in the elbow-joint between the distal humerus and proximal radius and ulna) in elbows injected with the combined (320 +5334) shRNA adenovirus when compared against the contralateral control (CLC) wings (Fig.4 B,C,D). Elbows independently injected with the 5334 and 320 shRNA viruses showed 13% and 14% reductions respectively in elbow-joint space when compared with corresponding contralateral controls (Fig.4 E,F). Area measurements of the non-chondrogenic space between the epiphyseal ends of the humerus, ulna and radius were performed using the area measurement tool of Image J software from NIH. Interzone area measurements of the injected and CLC wings resulting from all the treatments (shRNA control, 320 shRNA, 5334 shRNA and combined shRNA adenoviruses) were examined using the STATDISK software (Triola, 2005). Data analysis included calculation of means, standard deviations, and p-values for joint interzone areas of injected and uninjected contra-lateral control wings. Joint interzone area measurements from different wings could not be assumed to be statistically independent, and therefore mandated the use of conventional matched pair analysis feature of STATDISK (recommended by Dr. Said E. Said, statistics coordinator at ECU math department). The following null hypothesis was tested: There is no difference in the average synovial joint interzone area between the injected wing and the CLC wing. Statistical

significance was set at $p<0.05$. From this analysis, we saw that there was a statistically significant decrease in interzone areas for wings injected with all combinations of shRNA adenoviruses (Table 2). Wings injected with the negative-control shRNA virus showed no difference in interzone areas when compared to their contralateral counterparts. Table 1 shows the percentage of phenotypes resulting in reduced joint interzones for injected wings. More than 50% of viable embryos from each group of experimental adenovirus treatment, stained with Alcian Blue and Alizarin Red, showed a reduction in elbow joint spacing. The effects of versican knockdown on other factors involved in synovial joint morphogenesis were also examined.

Consequences on the expression patterns of key synovial joint markers in relation to versican knockdown were investigated using immunohistochemistry. For this purpose, embryos harvested at HH stages 34 or 36, following three to five days of infection, were LacZ stained and the injected and contralateral wings were either paraffin or cryostat sectioned. Antibody staining of wing sections showed altered expression patterns of key synovial joint markers such as collagen II, tenascin, link protein, CD-44 and hyaluronic acid (HA) in the joint interzone for the experimental adenoviral treated embryos. The most dramatic alterations in collagen II, tenascin and link protein expression were noticed for embryos treated with the combined shRNA adenovirus set (Figs. 6,10). Concurrent with versican knockdown in the articular chondrocytes lining the epiphyseal border of the humerus, where extensive adenoviral infection occurred for most injections, we noticed a dampening in the levels of collagen II, tenascin, and link protein at sites of transfection (Figs 6. A-F,10. A-D). The distal articular chondrocytes of the CLC humerus in Figure 6C shows defined collagen II staining along the border between the distal humerus and adjacent central interzone lamina. The adenovirus-injected wing in Fig.6D shows reduced collagen II staining at this border. Control adenovirus injection showed no differences in

the collagen II staining patterns between the CLC and injected wings along the distal humeral articular chondrocytes (Fig. 5 G,H).

In addition to reduced collagen II expression, versican silencing also led to attenuated expressions of tenascin and link protein in the articular cartilage matrix. Panels E and F in figure 6 show tenascin staining in the CLC and the injected wings respectively five days following combined adenovirus treatment. A clear reduction of tenascin can be seen in the distal humeral articular chondrocytes of the injected wing, where most adenoviral infection occurred. For the control shRNA treatment, there was no reduction in tenascin staining between the injected and CLC wings (Fig. 5 E,F). Similar effects were also observed for embryos treated independently with the 5334-adenovirus (Fig. 7).

Visible reductions in the expression of hyaluronan and CD44 occurred in the joint interzone on treatment with experimental shRNAs. On treatment with 320-shRNA adenovirus, there was a marked decrease in the expression of CD44 (Fig.8) and hyaluronan (Fig.9) in the joint interzone, especially along the maturing articular cartilage. Figure 8, B shows significant disorganization in the staining pattern of CD44 in the joint interzone when compared with the CLC wing. Similar disorganizations in hyaluronan expression are noticed in the interzone at sites of transfection (Fig. 9 C,D).

Interestingly, no significant difference in the number of cells undergoing apoptosis or proliferation at sites of shRNA transfection were noticed in the case of the injected elbows when compared with the CLC elbows at HH stage 36. Several specimens were sampled, and the number of cells undergoing proliferation at sites of transfection ranged from 3 to 6. In figure 13, at sites of transfection, there is no substantial difference between the injected elbow and corresponding areas in CLC elbows in either the 320-shRNA treatment (Fig. 13 A-D), or the

control (Fig. 13 E-H) treatment. Similarly, no major difference was observed for programmed cell death (Fig. 12).

Figure 1. Bar graph representing versican knockdown in chick embryonic fibroblast (CEF) cells 48 hours following infection with sh-RNA adenoviruses. Real time PCR results demonstrate 70% mRNA knockdown on infection with the 320-shRNA adenovirus and 50% knockdown with 5334-shRNA adenovirus. P-values obtained from Student t-test indicate significant reductions in versican mRNA levels when compared to the untreated control (unt).

Figure 1. Real time PCR assessment of versican knockdown by shRNA adenoviruses.

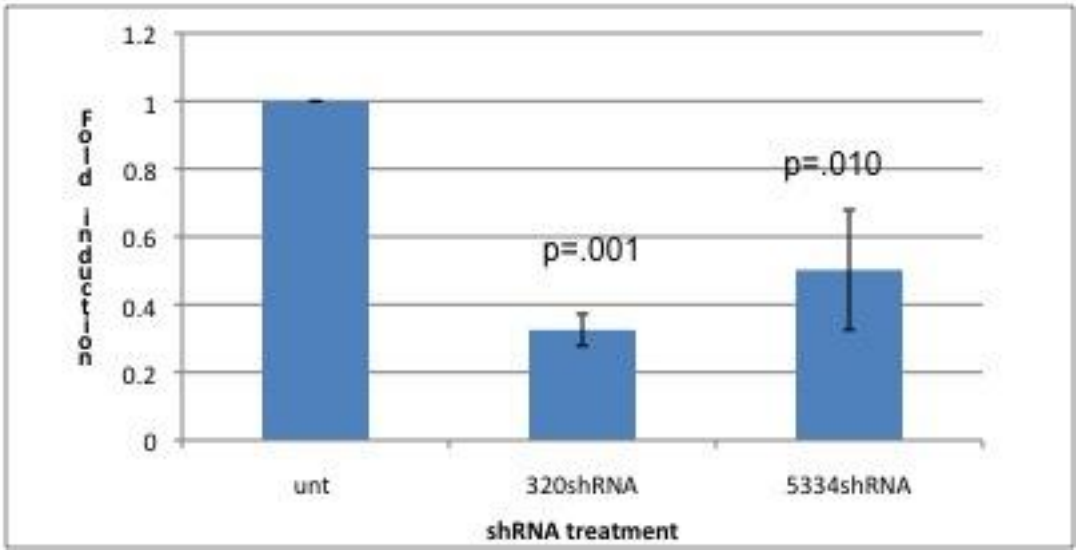

Figure 2. Real-time PCR assessment of versican mRNA knockdown *in ovo* on injection with a 1:1 combination of 320 and 5334-shRNA adenoviruses. Elbow joints from two sets of embryos were injected with the combined shRNA virus (Combined 1 and 2) and incubated for five days. Total RNA was extracted from the elbow joints, reverse transcribed, and quantitatively amplified against total RNA obtained from control sets injected with the control shRNA adenovirus. Data shows an average reduction of 65% in versican mRNA levels for the combined injections when compared with the control adenovirus.

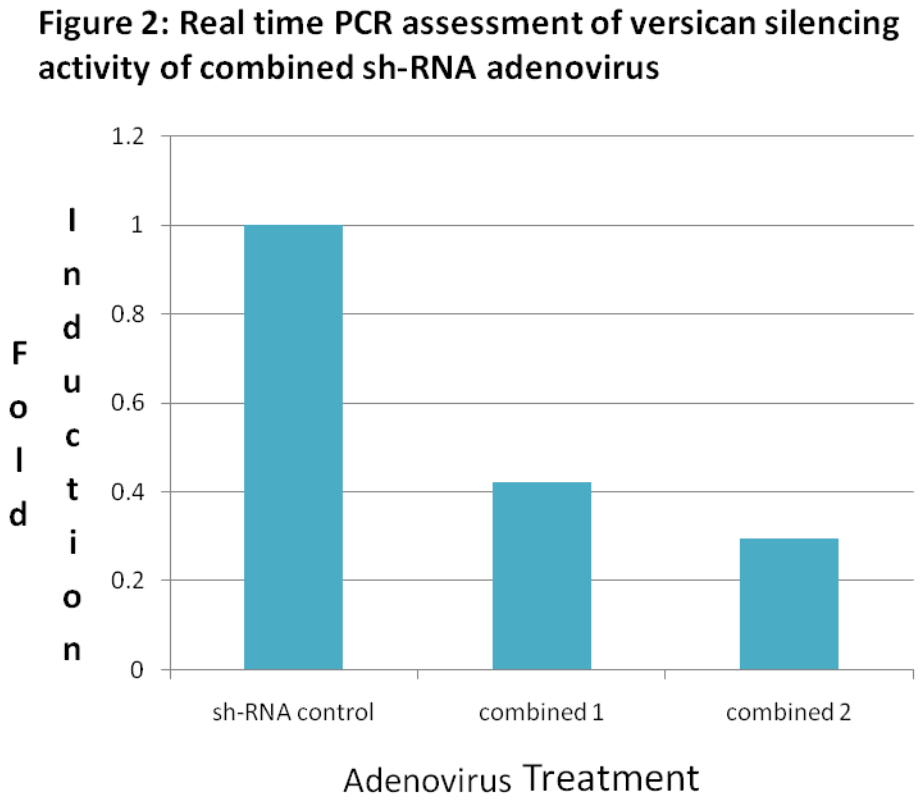

Figure 3. Immunohistochemical staining of paraffin sections through chick wing wrist joint at HH st36, 5 days following injection with 320-shRNA adenovirus. Protein-antibody staining demonstrates strong versican staining along the articular surface lining the distal ulna (**u**) and central lamina of the CLC wing carpal joint (**A**). A clear versican knockdown is visible in the carpal joint of wing injected with 320-shRNA adenovirus, especially among the articular chondrocytes lining the distal border of the ulna (**B**). Panels **C** and **D** are phase contrast images of panels **A** and **B** respectively. Panel **D** shows sites of shRNA transfection indicated by blue ß-galactosidase staining. Scale bar= 50µm.

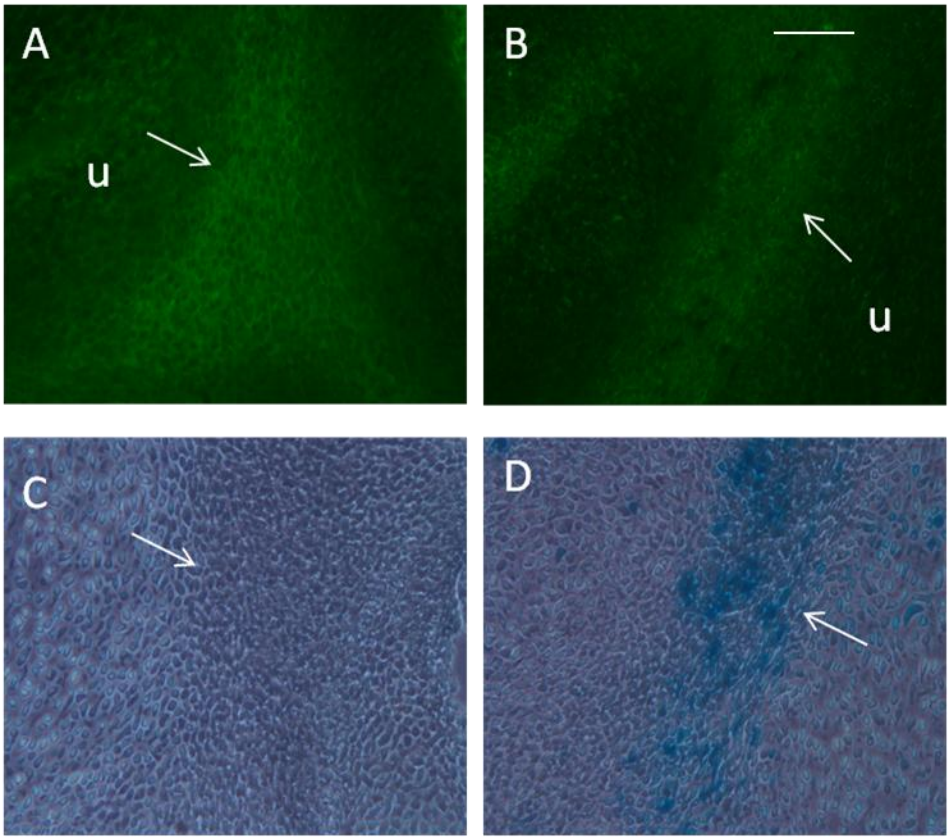

Figure 4. Whole-mount Alcian Blue/Alizarin Red staining of HH stages 36/37 chick wings, five days following injection with shRNA adenoviruses. **A**: Control adenovirus injections show no difference in synovial joint spacing. **B,C,D,E,F** indicate reduced elbow joint spacing on injection with combined (320,5334) (**B,C,D**), 5334 (**E**), and 320 (**F**)-shRNA adenoviruses. Arrows in each panel indicate injected elbow. The arrowhead in panel **F** shows an outline of the area measured for synovial joint spacing of all specimens. The red stain in panel **B** indicates β-galactosidase-Red Gal reactivity of the adenovirus indicating sites of shRNA transfection.

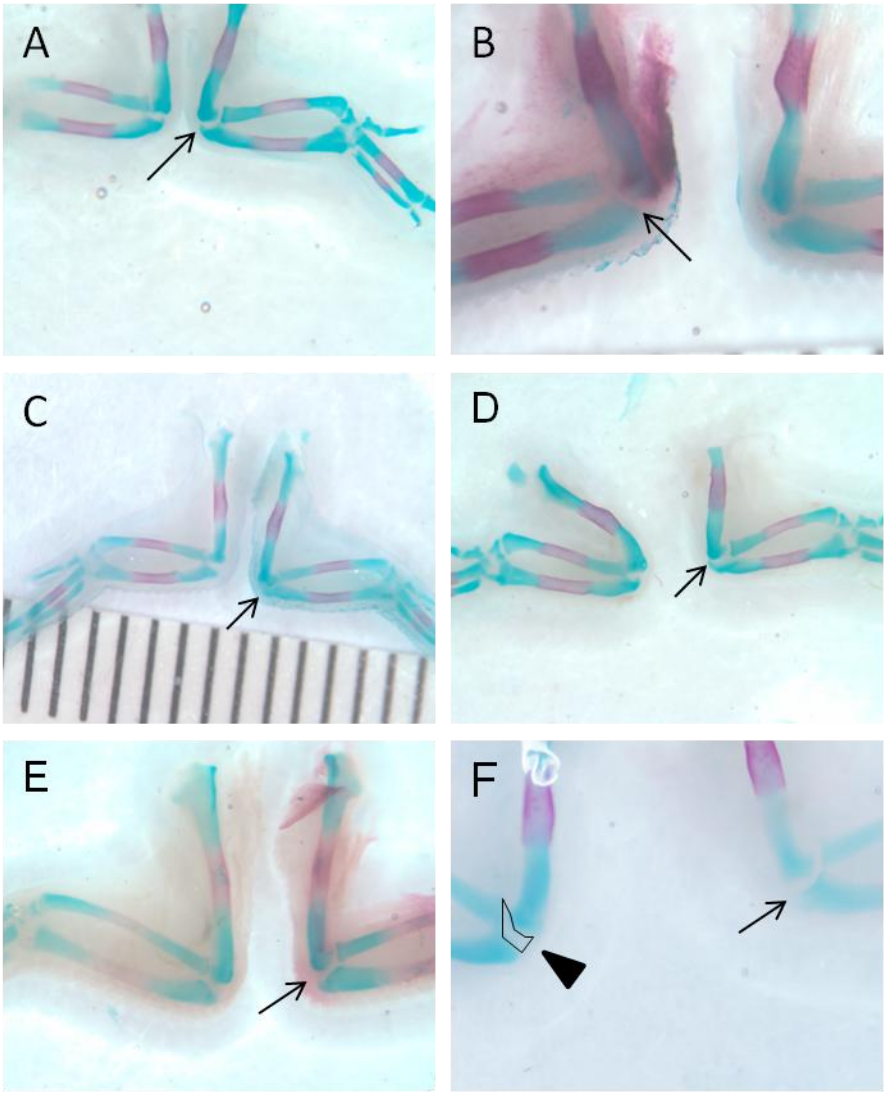

Figure 5. Immunohistochemical staining of paraffin sections through HH stage 36 chick elbows, five days following injection with control shRNA adenovirus. Panel **A** is a low magnification image of the contralateral control elbow interzone. Intense β-galactosidase (LacZ) staining indicating shRNA transfection can be seen in the synovial joint interzone between the humerus and ulna of the injected elbow (marked by arrow in panel **B**). Five days following injection, there was no noticeable decrease in the levels of versican, tenascin or collagen II expression (**D**,**F**, and **H**) in the elbow joint of the injected wing when compared to the expression levels of versican, tenascin, and collagen II (**C,E** and **G**) respectively in the contralateral control wing. Scale bar for panels **A,B,C,D,G**, and **H** = 100µm. Scale bar for panels **E** and **F** = 50µm

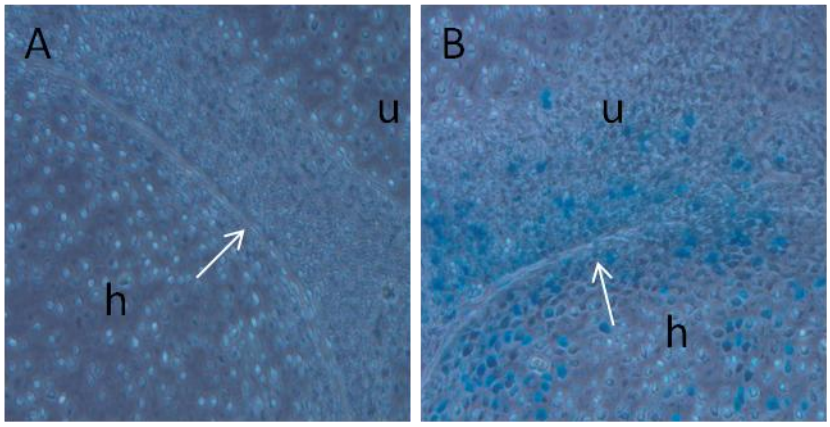

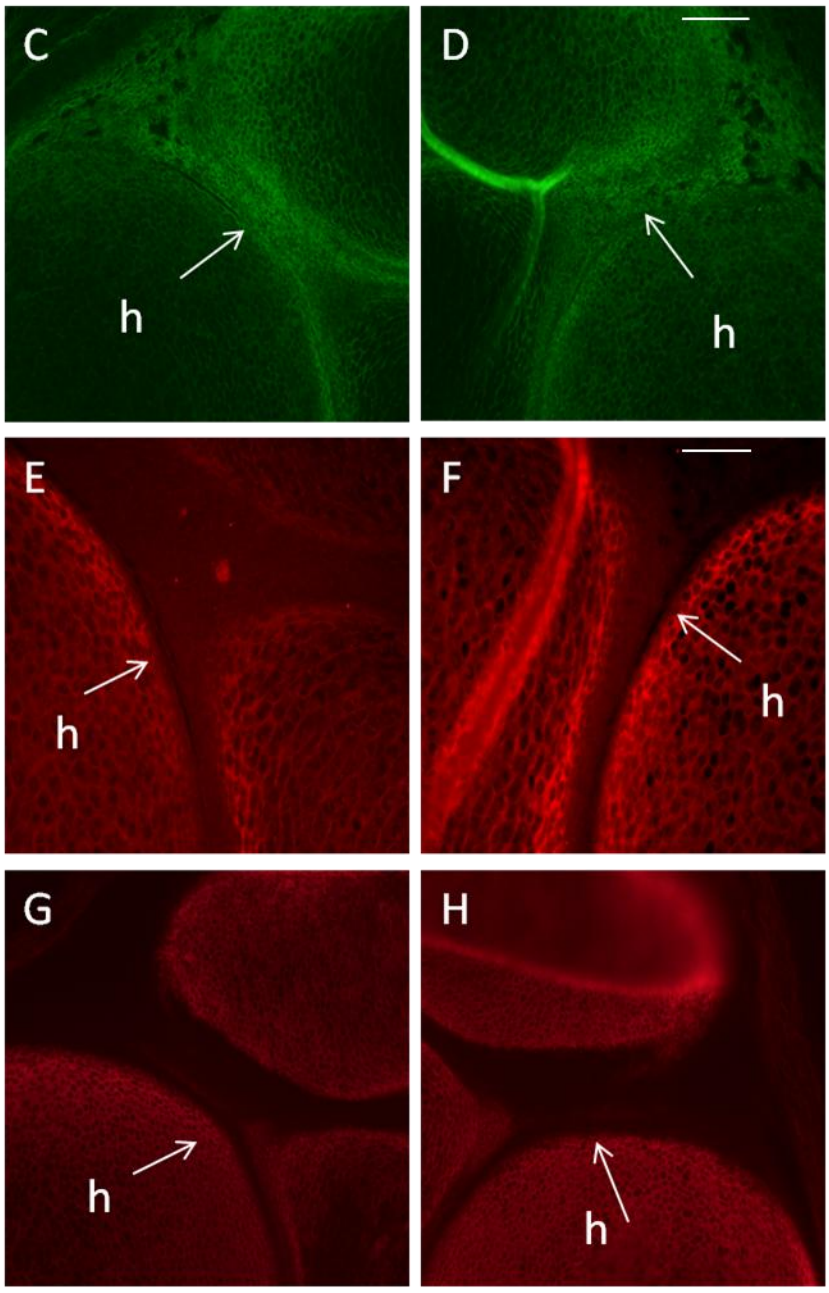
C
h
D
h
E
h
F
h
G
h
H
h

Figure 6. Immunohistochemical staining of paraffin sections through HH stage 36 chick elbows, five days following injection with the combined (320+5334) shRNA adenovirus. Panels **A** and **B** are low magnification images of panels **C** and **D** respectively. Panels **D**, **F**, and **H** indicate reductions in the levels of collagen II, tenascin and versican in the injected elbow joint when compared to corresponding CLC elbow (**C**,**E**,**G**). Defined collagen II staining can be seen in the articular cartilage matrix bordering the distal humerus in CLC wing (indicated by arrowhead) (**C**). Collagen II expression is less intense among the distal humeral articular chondrocytes of the injected wing (**D**). Versican expression is also lower in the joint interzone of the injected wing (**H**), especially among the humeral articular chondrocytes, when compared to the CLC wing (**G**). Arrows indicate areas of reduced marker expression. Panels **I** and **J** are phase contrast images of panels **G** and **H** respectively. The arrow head in panel **J** shows the sites of shRNA transfection. Scale bar for panels **C**-**J** = 50μm. Scale bar for panels **A** and **B** = 100μm.

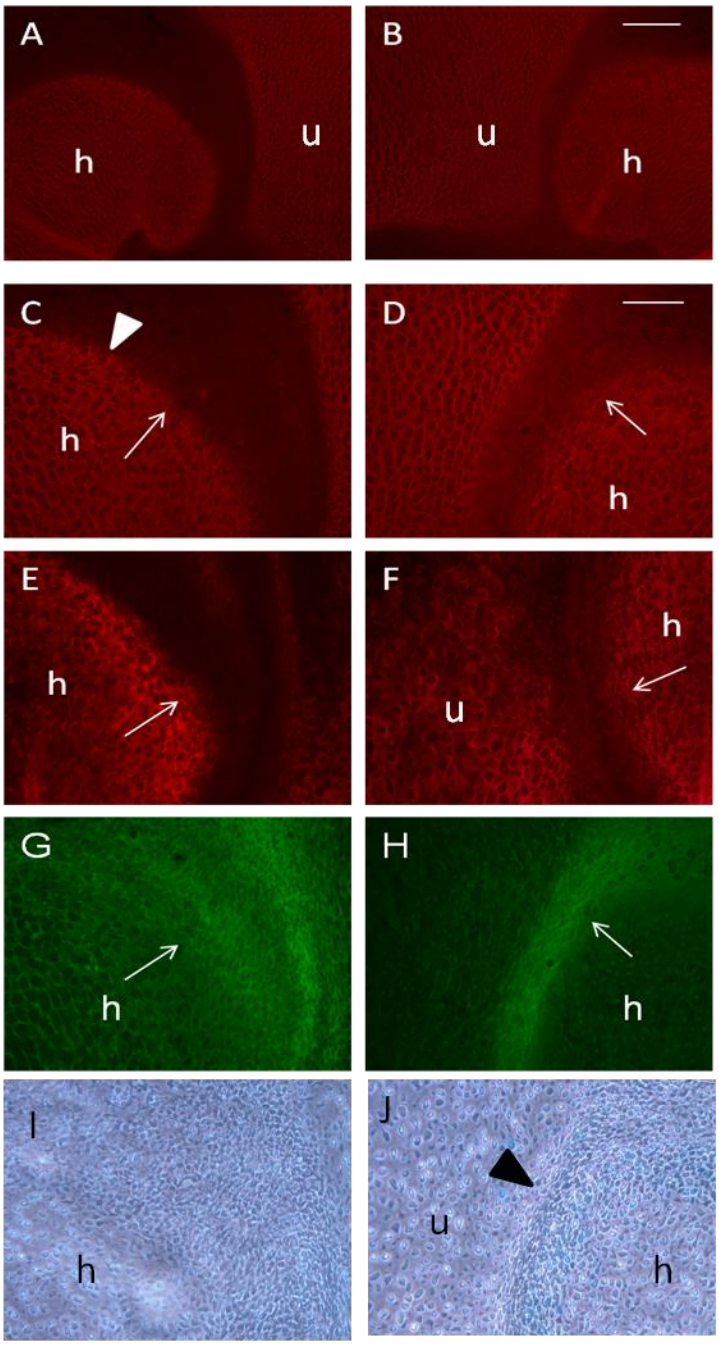
A
h
u
B
u
h
C
h
D
h
E
h
F
h
u
G
h
H
h
I
h
J
u
h

Figure 7. Immunohistochemical staining of paraffin sections through HH stage 36 elbows, 5 days following injection with the 5334-shRNA adenovirus. Panel **A** is a low magnification bright field image showing the sites of shRNA transfection in the injected wing. Panel **C** shows reduced tenascin expression in the articular cartilage matrix of the distal humerus of the injected humero-ulnar joint when compared to the CLC joint (**B**). This corresponds with reduced versican expression seen in the articular cartilage of the injected wing (**E**) when compared with that of the CLC wing (**D**). Panel **A** in addition to panel **E** further shows that versican silencing has occurred at the sites of sh-RNA transfection. Panels **H** and **I** are higher magnifications of the boxed areas of panels **F** and **G** respectively. Panel **I** shows reduced collagen II expression among the articular chondrocytes of the injected wing. Very defined collagen II staining can be seen along the articular surface of the distal humerus in panel H, especially in the transition between the distal humerus and the adjacent interzone lamina. Scale bar for panels A-G= 100μm, and for panels H-I = 50μm.

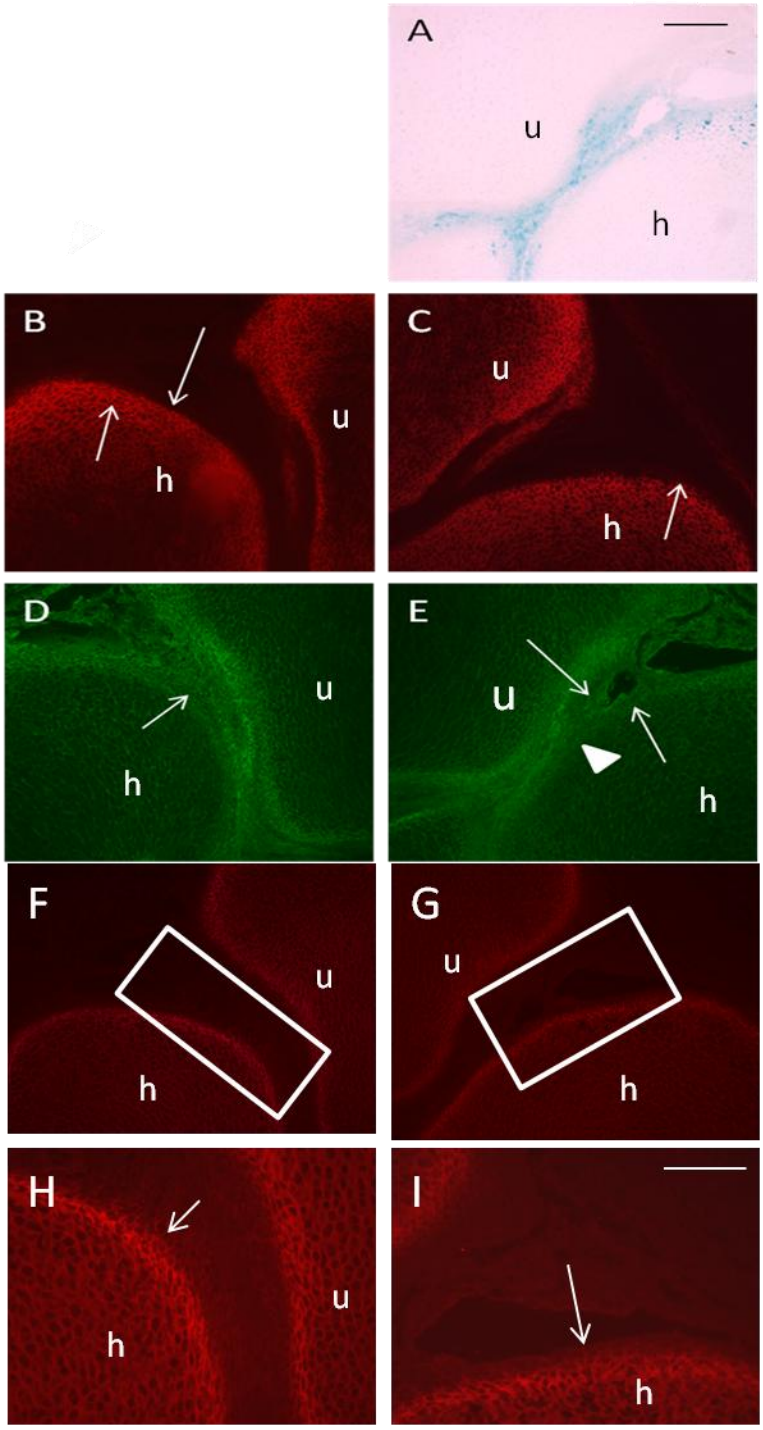
A
u
h
B
u
h
C
u
h
D
u
h
E
u
h
F
u
h
G
u
h
H
u
h
I
h

Figure 8. Immunohistochemical staining of cryostat sections through HH stage 34 elbows, 3 days following injection with 320-shRNA adenovirus. Panels **A** and **C** show defined extracellular CD44 staining in the joint interzone of the CLC wing lining the articular cartilage. Panels **B** and **D** show less defined and reduced CD 44 extracellular staining in the joint interzone of the injected wings. Note that in the injected wing the interzone tissue seems loosened and the cells seem to be less densely packed based on the fluorescence and phase contrast images. Panels **C** and **D** are higher magnification images of panels **A** and **B**. Panels **E** and **F** are phase contrast images of panels **C** and **D** respectively. Arrowhead in panel **F** indicates area of reduced cell densities at sites of sh-RNA transfection indicated by the ß-galactosidase staining. Scale bar for panels **A** and **B** = 100μm and for panels **C-F** = 50μm

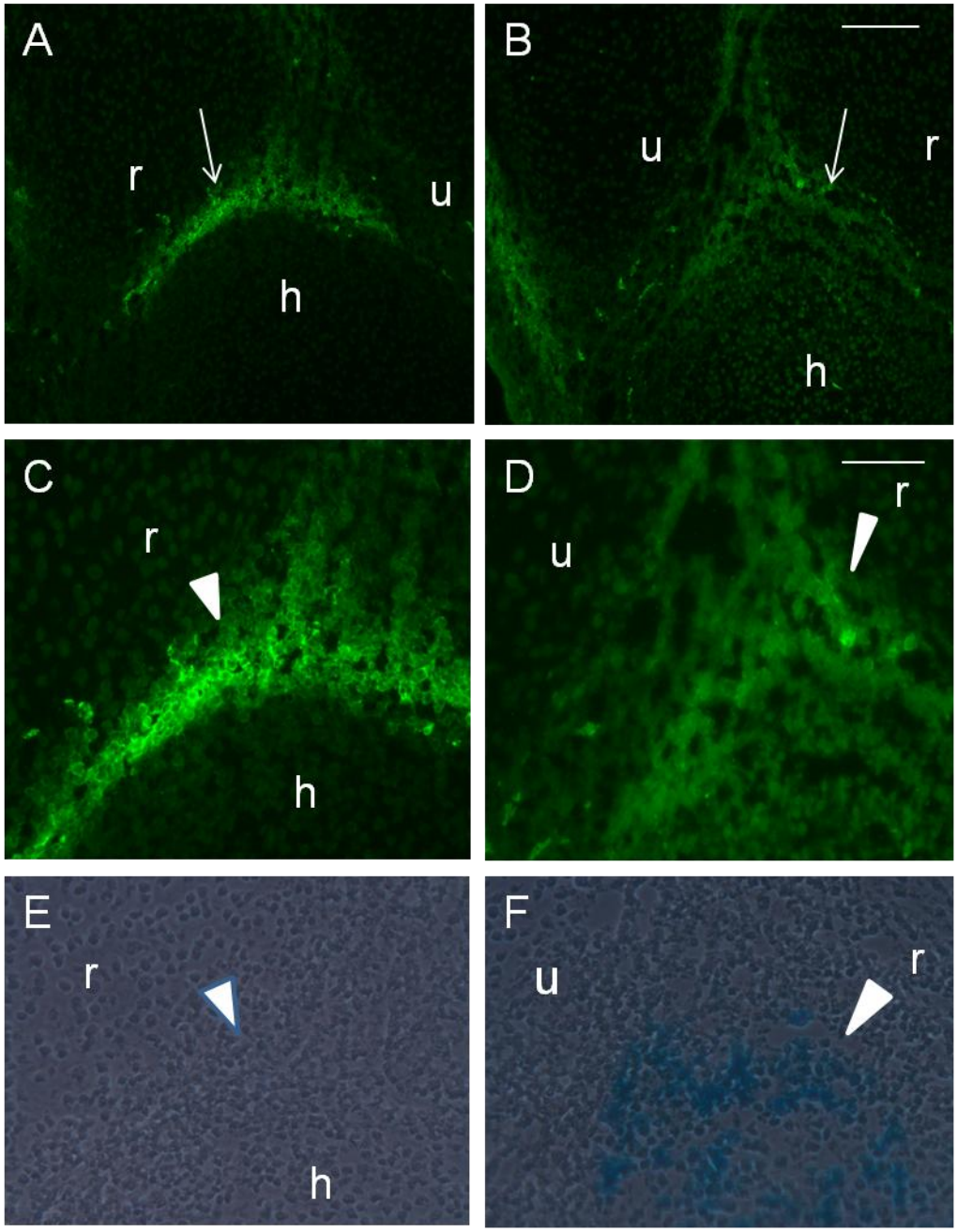
A
r
u
h
B
u
r
h
C
r
h
D
r
u
E
r
h
F
u
r

Figure 9. Immunohistochemical staining of cryostat sections through HH stage 34 elbows, 3 days following injection with 320 sh-RNA adenovirus. Panels **C** and **D** are higher magnification images of the boxed areas in panels **A** and **B** respectively, which represents the joint interzone space between the humerus (**h**) and ulna (**u**) for the injected (panels **A**, **C**, **E** and **G**) wing and the CLC wing (panels **B**, **D** and **F**). Robust HA staining is seen in the humero-ulnar joint interzone in panel **D** whereas almost no specific extracellular HA staining is apparent in the humero-ulnar joint of the injected wing at sites of sh-RNA transfection (panels **E** and **G**). Panel **G** is a bright field image of panel **E**. Scale bar for panels **A** and **B** = 100μm and for panels **C-G** = 25μm.

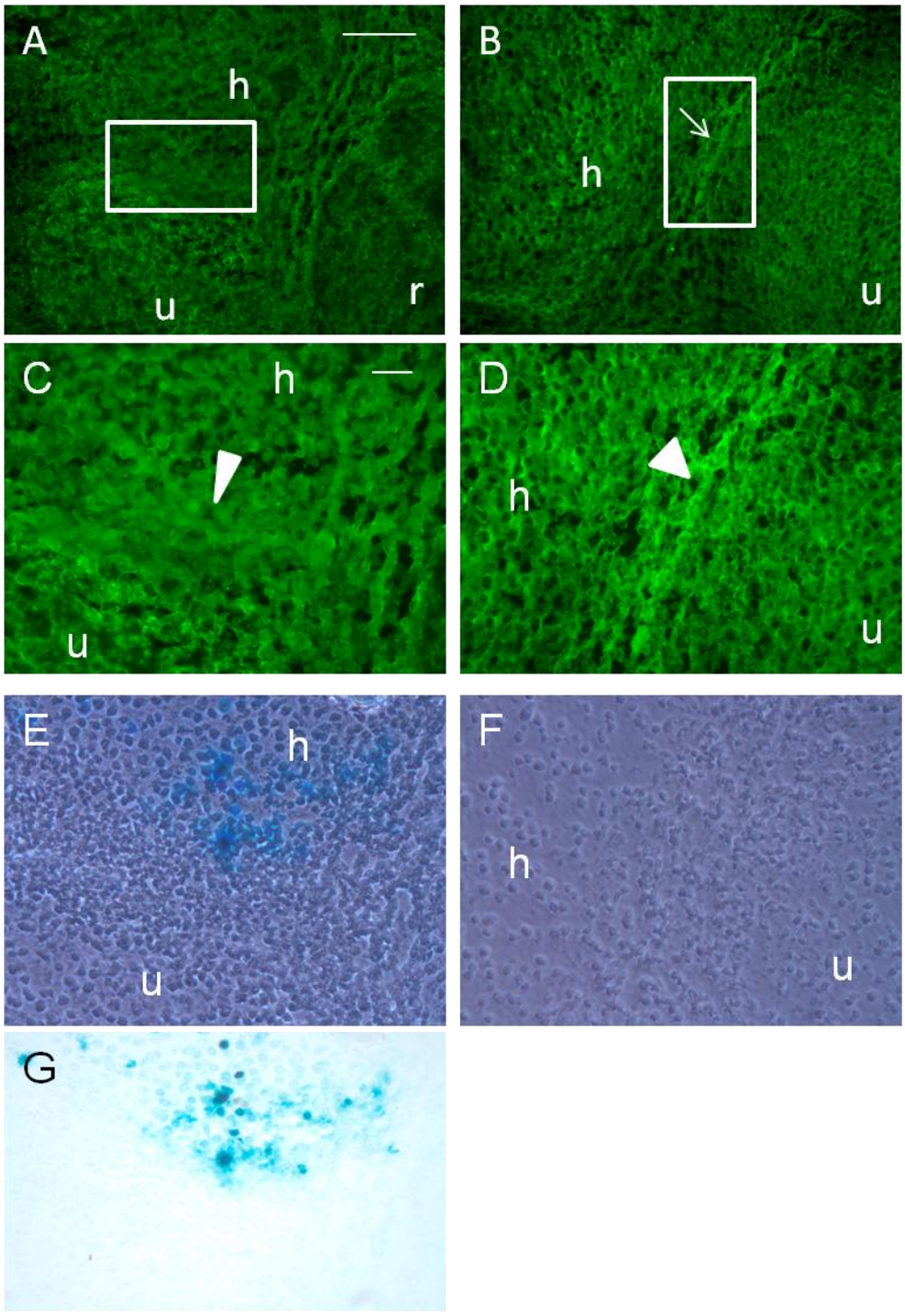
A
h
u
r
B
h
u
C
h
u
D
h
u
E
h
u
F
h
u
G

Figure 10. Immunohistochemical staining of paraffin sections through HH stage 36 elbows, 5 days following injection with the combined (320+5334) sh-RNA adenovirus. Panels **C** and **D** are low magnification images of the boxed areas in panels **A** and **B** respectively. Panel **D** shows a reduction in link protein expression in the injected wing at the articular surface of the distal humerus (indicated by arrowhead), where most transfection occurred (Panels **F** and **G**). Panels **F** and **G** are phase contrast and bright field images of panel **D** showing the sites of transfection. The red color in the phase and bright field images indicate ß-galactosidase reactivity. Panel **E** is a phase contrast image of panel **A**. Scale bar=100μm (**A,B**) and 50μm (**C-G**).

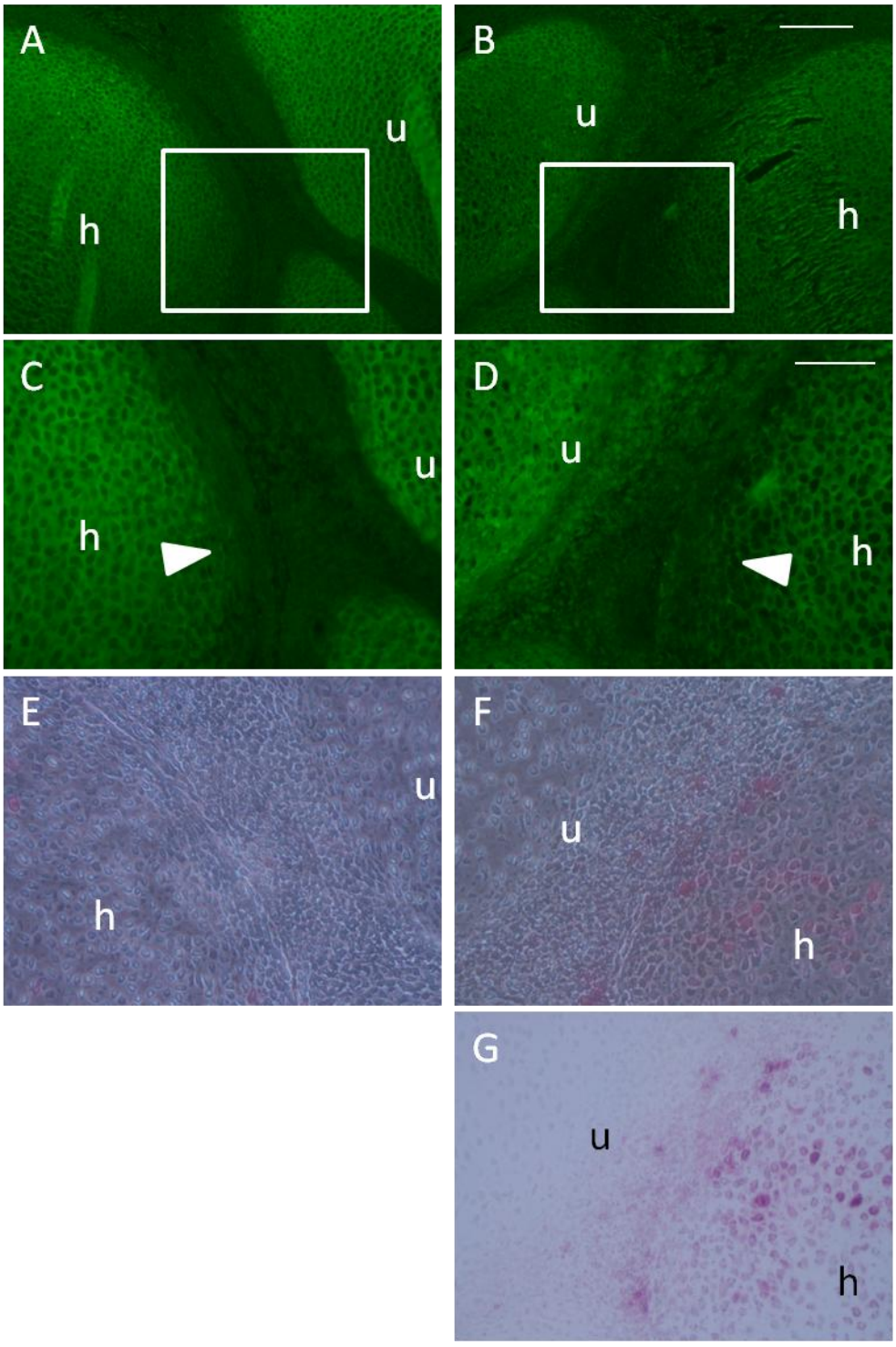
A
u
h
B
u
h
C
u
h
D
u
h
E
u
h
F
u
h
G
u
h

Figure 11. Immunohistochemical staining of paraffin sections through HH stage 36 elbows, 5 days following injection with control sh-RNA adenovirus. Panels **C** and **D** are high magnification images of the boxed areas in panels **A** and **B** respectively. Note that there is no difference in the level of link protein expression in the distal humeral articular chondrocytes (arrow head) between the injected elbow and the ClC elbow. Panel **F** is a phase contrast image of panel **D** showing the sites of sh-RNA transfection. Scale bar= 100μm (**A,B**); 25μm (**C-F**).

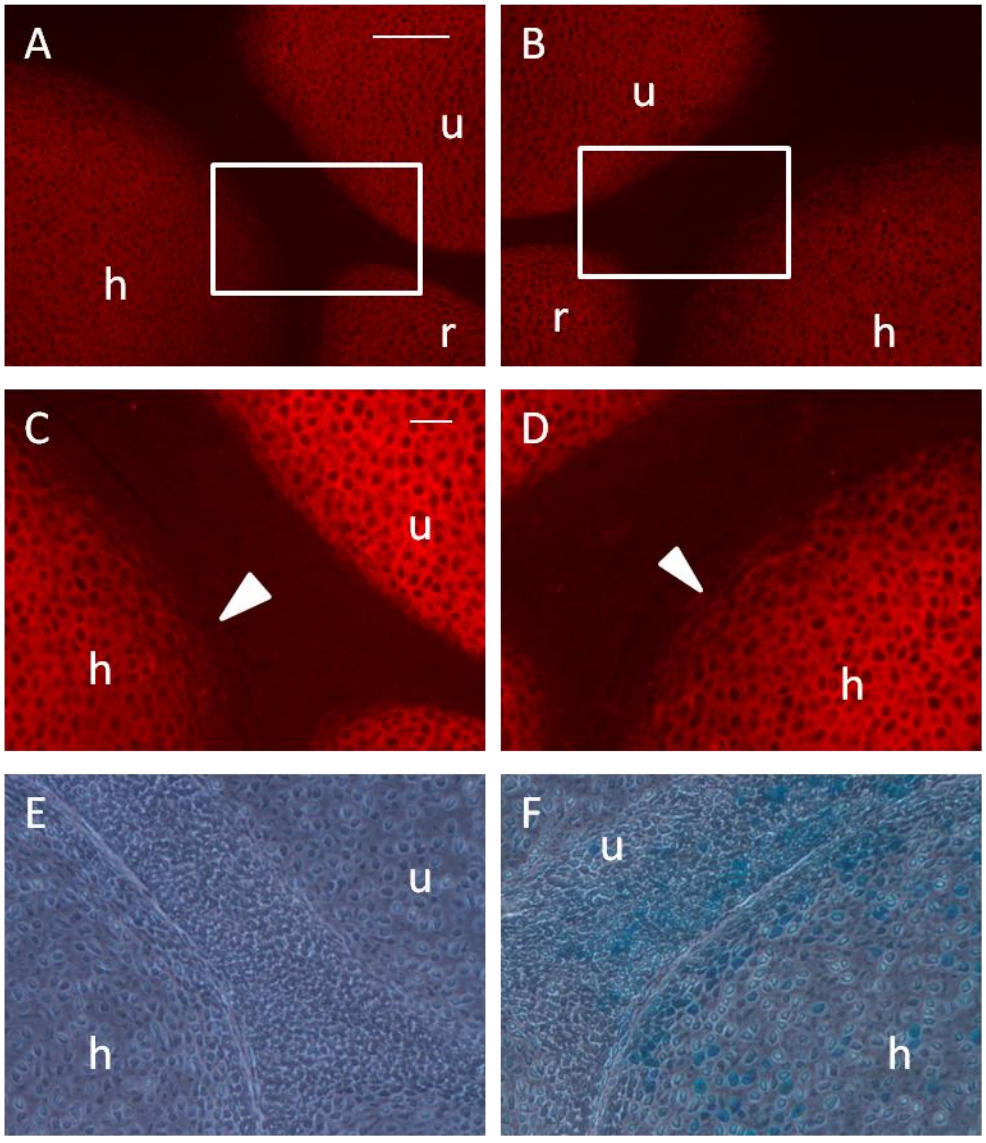

Figure 12. TUNEL Assay apoptosis staining of paraffin sections through HH stage 36 elbows, 5 days following injection with control-shRNA adenovirus (**A**) and combined shRNA adenovirus(**B**). Panel **C** shows the contralateral contol counterpart for **B**. The boxes in the panels enclose areas of sh-RNA transfection that was used to count the number of apoptotic cells (stained dark brown). The boxed area in panel **B** contained about 9 apoptotic cells, whereas the boxed area in panel **A** contained 11 apoptotic cells. No major difference was seen in the number of apoptotic cells between the control sh-RNA transfected wing and combined sh-RNA transfected wing. Scale bar= 100μm for all panels.

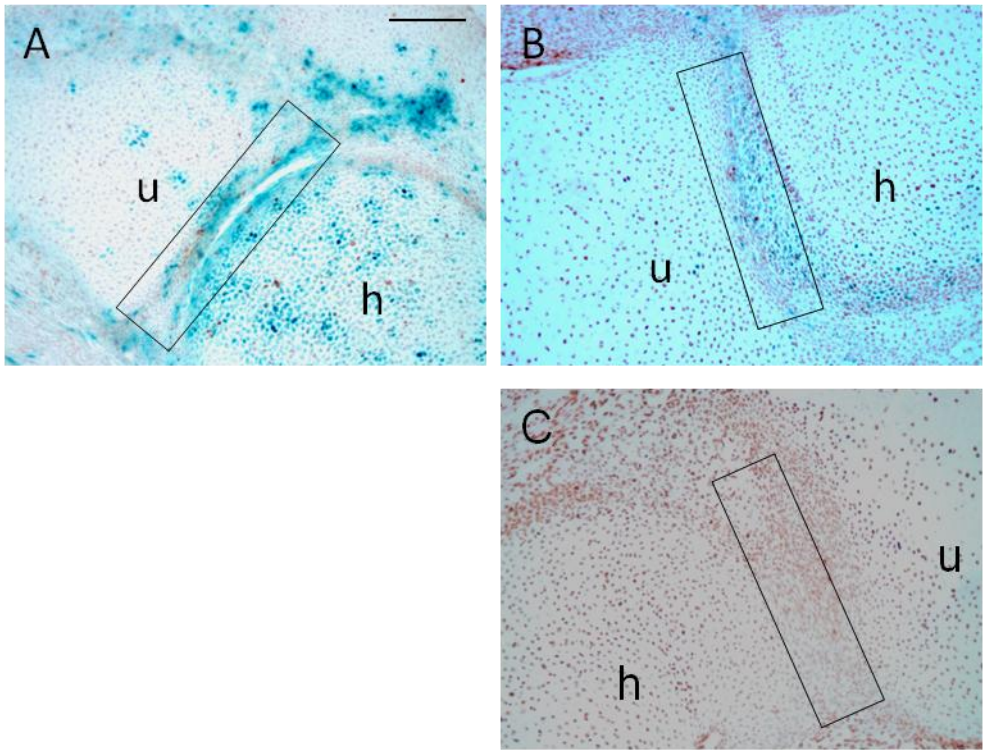

Figure 13. Phosphohistone antibody staining of paraffin sections through HH stage 36 elbows, 5 days following injection with 320 (**A-D**) and control sh-RNA adenoviruses (**E-H**). Boxed area in panel **B** indicates almost the same number of histone positive cells as in the boxed area in the CLC wing (**A**). The difference in the number of histone-positive cells between the injected and CLC wings is also not apparent in the embryo injected with the control sh-RNA adenovirus. There seems to be almost the same number of histone positive cells in both the injected joint interzone (**F**) as well as the CLC interzone (**E**). Panels **G** and **H** are phase contrast and bright field images respectively of the CLC wing and the injected wing. Panel **H** shows thorough transfection of the control sh-RNA in the humero-ulnar interzone. Scale bar= 50μm (C). Scale bar for all other panels = 100μm.

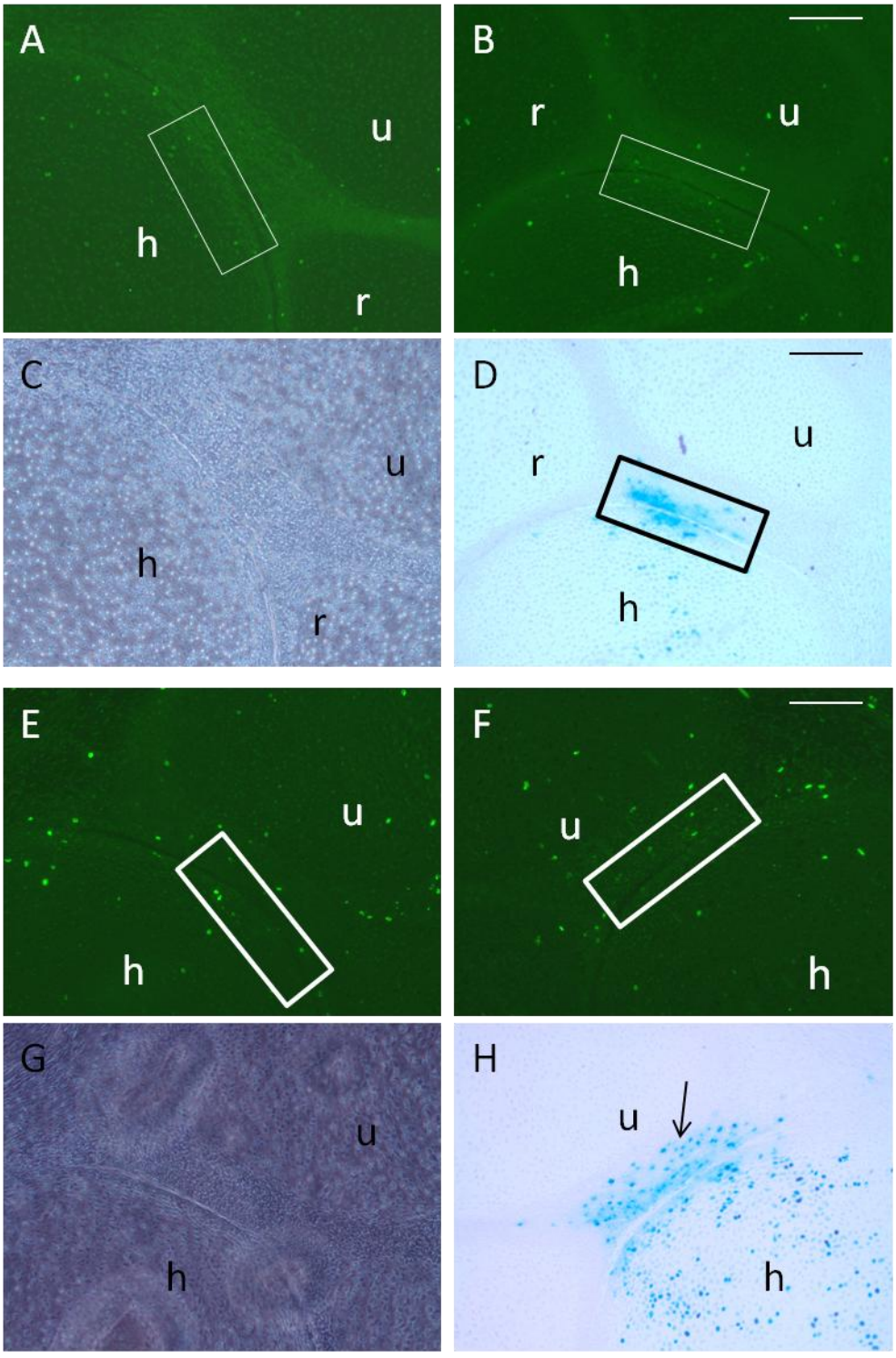
A
u
h
r
B
r
u
h
C
u
h
r
D
u
r
h
E
u
h
F
u
h
G
u
h
H
u
h

Table 1. Elbow-joint phenotypes resulting from morphometric analysis of Alcian Blue/Alizarin Red stained whole embryos (HH 36-37) injected with control-shRNA, 320-shRNA, 5334-shRNA and combined (320+5334 shRNAs) at HH24-25.

Adenovirus	Number of Embryos Injected (n)	Embryos with Reduced, Interzone Areas	Percentage with phenotype
control-shRNA	6	0	0%
320-shRNA	7	4	57%
5334-shRNA	7	4	57%
320+5334 shRNA	9	5	55%

Table 2. Estimated interzone areas in square-millimeters (mm^2) at HH 36-37. Mean matched-pair analysis was performed to confirm whether differences between average interzone areas of the injected versus CLC wings were statistically significant;. Pvalues < 0.05 was deemed to be significant.

Adenovirus (shRNA)	CLC	Injected	P-value
control-shRNA	0.120±0.03	0.120±0.04	NS
320-shRNA	0.124±0.03	0.107±0.02	0.03
5334-shRNA	0.121±0.02	0.105±0.02	0.041
320+5334	0.113±0.02	0.097±0.03	0.02

Discussion

Synovial joint formation is a complex yet increasingly better understood process. Proper joint morphogenesis critically hinges on a series of physical and molecular processes that involve the flattening of joint interzone cells followed by joint cavitation, which is known to be facilitated by the extracellular accumulation of the glycosaminoglycan hyaluronan (HA) in joint interzone tissue (Pitsillides et al. 1995, Craig et al. 1990). A study utilizing chick embryo wings recently demonstrated that the hyalectin proteoglycan versican is continuously expressed in the joint interzone during early stages of joint morphogenesis. Interestingly, at progressively later stages (HH stage 41 and onward) it was shown that versican activity tends to decline in the joint epiphysis, but is persistent among the articular chondroctyes lining the joint interzone (Shepard et al. 2007).

The intent of this study was to better understand matrix versican's functions during synovial joint establishment *in vivo*. We approached this question by attempting to analyze the morphologic and molecular consequences of ectopically silencing versican protein levels in the synovial joint during early stages of chick elbow joint morphogenesis (HH stage 25) and then assessing the effects at progressively later stages (HH stages 34 and 36). We hypothesized that knocking down versican would lead to a distortion of synovial joint morphology brought about by alterations in the expression patterns of other key synovial joint markers. To test our hypothesis, we used adenovirally-encoded shRNAs previously prepared in our laboratory and *in-ovo* microinjection techniques. Alcian Blue/Alizarin Red staining of HH stage 36-embryo wings resulted in overall 13-14% reductions in the area of the nonchondrogenous space between opposing epiphyseal ends in the shRNA-treated elbows when compared with corresponding contralateral controls. In addition to this diminished elbow spacing, we noticed reduced

expression and disorganized distributions of other synovial joint and articular cartilage markers including collagen II, tenascin, CD44, HA, and link protein at sites of shRNA transfection.

Interestingly, a very recent study utilizing a conditional versican knockout mouse model reported a 'tilting' of the joints in the digits of the hindlimb autopod. This 'tilting' phenotype was ascribed to close packing of mesenchymal cells at the joint interzone, in addition to disruptions of chondrocyte columns in the digits. In the mutant mouse strain, the authors observed hypertrophy of chondrocytes, and slight delays in chondrocyte differentiation in the digits when compared with hindlimb autopod of control mice fully expressing versican. This joint-tilting phenotype and delays in chondrogenesis were further attributed to disruptions in versican's localization of TGFß extracellularly at the sites of impact. Interestingly, in their study, the authors did not notice any phenotypic difference in the more proximal elbow or knee joints. The authors believe that this 'tilting' phenotype was only observed in the hindlimb autopod, since TGF-ß signaling is more prevalent in that area (Choocheep et al. 2010).

In our study utilizing a knockdown system, we chose to analyze the impacts of transient versican silencing on the more proximal elbow joints. This was done as a precaution, since attempting to inject into the autopod could potentially damage the AER and lead to mechanically induced skeletal deformities (Saunders 1948). Five days after injecting presumptive elbows with shRNAs targeting versican, we noticed marked reductions in the expression of extracellular collagen II among developing articular chondrocytes concomitant with decreased versican levels at sites of transfection. Since collagen II is a well-established marker for chondrocyte maturity and differentiation (Linsenmeyer et al, 1973), a decrease in collagen II among the presumptive articular region could manifest as delay in establishing articular chondrocyte maturity and permanence.

In addition to reductions in collagen II, we also noticed observable decreases in expression of link protein among the early articular chondrocytes of the developing joint interzone at sites of versican knockdown. Link protein, in addition to collagen II and aggrecan, is a major structural feature of maturing cartilage. Link protein's interaction with aggrecan and hyaluronan to from a stabilized aggrecan-HA-link protein complex to promote chondrocyte stability has been previously recorded (Hardingham 1979). Recent findings interestingly indicate that link protein shows greater affinity towards interactions with the G1 domain of versican than the G1 domain of aggrecan to form more stabilized versican-HA-link protein ternary complexes (Shi et al. 2004).

Not surprisingly, a previous study utilizing link protein knockout mice reported cartilage deficiencies and disorganizations of chondrocyte columns during epiphyseal-growth plate development. This disorganization of the columns was attributed to weakened depositions of proteoglycan-aggregates in the extracellular matrix needed for maintaining cartilage integrity. The study also reported decreased chondrocyte sizes. Intriguingly, the authors did not notice any differences in cell proliferation resulting from the absence of link protein. The authors also noted a diminishing in aggrecan staining among the chondrocytes, and an unwillingness of pre-hypertrophic chondrocytes to differentiate to the hypertrophic state (Watanabe and Yamada 2003). In our examinations of elbow joints impacted by versican knockdown, we did not notice any overt signs of chondrocyte hypertrophy in or near the elbow. From our demonstrations of reductions in collagen II and link protein levels concurrent with curtailed versican expression, in conjunction with the findings of Watanabe and Yamada, it seems a viable argument that versican plays a pivotal role in preserving the chondrocytic characteristics of articular cartilage by

facilitating proper link protein functioning and possibly preventing articular chondrocytes from decreasing in size.

In our study, the expression pattern of glycoprotein tenascin was also visibly reduced in response to versican knockdown in the elbow joint interzone, mainly in the presumptive articular cartilage matrix lining the epiphyseal ends of the distal humerus. A previous study demonstrated that in cartilaginous areas where reductions in tenascin expression occur, those areas become particularly vulnerable to chondrocyte maturation and hypertrophy, eventually leading to osteogenesis (Pacifici et al. 1993). From our findings and that of the study just mentioned, it seems reasonable to speculate that if versican silencing is allowed to continue in the joint interzones, then the articular chondrocytes of those joints may have higher chances of hypertrophy and eventual osteogenesis.

In addition to the factors discussed previously, hyaluronan (HA) and its cell surface receptor CD44 are also known key players in synovial joint morphogenesis. Furthermore, a recent publication has shown that versican is involved in regulating HA and CD44 activities in extracellular signal transduction pathways (Suwan et al. 2009). Another study using Hyaluronan synthase 2 (*Has 2*) knockout mice led to hyaluronan deficiencies in the limb. Additionally, defective synovial joint cavities were observed, along with defects in chondrocyte maturation confirmed by reductions in extracellular aggrecan. Moreover, the synovial joints of older mice showed increased cell packing and the joints were observed to be wider than usual (Matsumoto et al. 2009). Defective joints were also reported in cases where the interaction between hyaluronan and CD44 was interrupted using hyaluronan oligisaccharides (Dowthwaite et al. 1998). In our study investigating effects of versican knockdown, we noticed visible deficiencies in both CD44 and hyaluronan expression in the elbow joint interzone consistent with

versican silencing. This can be a cause for disruptions in interactions between hyaluronan and CD44. In our study, we reported reductions in the non-chondrogenic spacing between opposing epiphyseal ends comprising the elbow joint. This reduction in space is possibly due to the packing of mesenchymal cells of the central lamina. Also in our situation, we did not notice any significant difference in the cell proliferation, or apoptosis between shRNA treated and control elbows. Thus from our examination of the various factors impacted by versican knockdown in the joint interzone, it seems that our reduced joint-space phenotype is due to a collective effect resulting from the altered expression of various synovial joint factors impacted by versican silencing.

References

Archer CW, Morrison H, Pitsillides AA. 1994. Cellular aspects of the development of diarthrodial joints and articular cartilage. J. Anat. 184: 447-456.

Archer CW, Dowthwaite GP, Francis-West P. 2003. Development of Synovial Joints. Birth Defects Research. 69: 144-155.

Aspberg AR, Miura S, Bourdoulous M, Shimonaka D, Heinegard MS, Ruoslahti E, Yamaguchi Y. 1997. The C-type lectin domains of lecticans, a family of aggregating chondroitin sulfate proteioglycans, bind tenascin-R by protein-protein interactions independent of carbohydrate moity. Proc. Natl. Acad. Sci. 94: 10116-10121.

Capdevila J, Belmonte JCI. 2001. Patterning Mechanisms Controlling Vertebrate Limb Development. *Annu. Rev. Cell Dev. Biol*. 17:87-132.

Craig FM, Bentley G, Archer CW. 1987. The spatial and temporal pattern of collagens I and II and keratin sulphate in the developing chick metatarsophalangeal joint. Development. 99: 383-91.

Craig FM, Bayliss MT, Bentley G, Archer CW. 1990. A role for hyaluronan in joint development. J.Anat. 171: 17-23.

Choocheep K, Hatano S, Takagi H, Watanabe H, Kimata K, Kongtawelert P, Watanabe H. 2010. Versican Facilitates Chondrocyte Differentiation and Regulates Joint Morphogenesis. J. Biol. Chem. 285: 21114-25.

Cohn MJ, Patel K, Krumlauf R, Wilkinson DG, Clarke JD, Tickle C. 1997. Hox9 genes and vertebrate limb specification. *Nature* 387: 97-101.

Cohn MJ, Tickle C. 1999. Developmental basis of limblessness and axial patterning in snakes. *Nature* 399: 474-79.

Crossley PH, Monowada G, MacArthur CA, Martin GR. 1996. Roles for FGF-8 in the induction, initiation, and maintenance of chick development of the tetrapod limb. Cell 84: 127-136.

De Boever S, Vangestei C, De Backer P, Croubels S, Sys S. 2008. Identification and validation of housekeeping genes as internal control for gene expression in an intravenous LPS inflammation model in chickens. Vet. Immunol. Immunopathol. 122: 312-317.

Dessau W, von der Mark H, von der Mark K, Fischer S. 1980. Changes in the patterns of collagens and fibronectin during limb-bud chondrogenesis. J. Embryol. exp. Morph. 57:51-60.

Dowthwaite GP, Edwards JCW, Pitsillides AA. 1998. An essential role for the interaction between hyaluronan and hyaluronan binding proteins during joint development. J. Histochem. Cytochem. 46: 641-651.

Edwards JC, Wilkinson LS, Jones HM, Soothill P, Henderson KJ, Worrall JG, Pitsillides AA. 1994. The formation of human synovial joint cavities: A possible role for hyaluronan and CD44 in altered interzone cohesion. J. Anat. 185(Pt.2): 355-367.

Fallon, J.F. and G.M. Crosby. 1977. Polarizing zone activity in limb buds of amniotes. *In* D.A. Ede, J.R. Hinchliffe and M. Balls (eds.), *Vertebrate Limb and Somite Morphogenesis*. Cambridge University Press, Cambridge. pp. 55-59.

Fell HB. 1925. The histogenesis of cartilage and bone in the long bones of the embryonic fowl. Journal of Morphology 40: 417-459.

Fell H, Canti R. 1934. Experiments on the development in vitro of the avian knee joint. Proc. R. Soc. 116: 316-327.

Guo X, Day TF, Jiang X, Garrett-Beal L, Topol, L, Yang Y. 2004 Wnt/beta-catenin signaling is sufficient and necessary for synovial joint formation. Genes Dev. 18: 2404-2417.

Hall BK, Miyake T. 1996. Divide, accumulate, differentiate: cell condensation in skeletal development revisited. Int. J. Dev. Biol. 39: 881-93.

Hamburger V, Waugh M. 1940. The primary development of the skeleton in nerveless and poorly innervated limb transplants of chick embryos. Physiol.Zool. 13: 367-384.

Hamburger V, Hamilton HL. 1951. A series of normal stages in the development of the chick embryo. *J. Morphol*. 88:49-92.

Hardingham TE. 1979. The role of link-protein in the structure of cartilage proteoglycan aggregates. Biochem J. 177: 237-247.

Harrison RG. 1918. Experiments on the development of forelimb of Ambystoma, a self differentiating equipotential system. J. Exp. Zool. 25: 413-461.

Hartmann C, Tabin CJ. 2001. Wnt-14 plays a pivotal role in inducing synovial joint formation in the developing appendicular skeleton. Cell. 104: 341-351.

Hay ED. 1991. Cell biology of extracellular matrix., 2nd edn New York Pienum Press.

Hertwig O. 1925. Haploidkernige Transplante als Organisatoran diploidkeniger Extremitaten be Triton. Anat. Anz. [Suppl.] 60: 112-118.

Hinchliffe, J.R. 1991. Developmental approaches to the problem of transformation of limb structure in evolution . In J.R. Hinchliffe (ed.), Developmental Patterning of the Vertebrate limb. Plenum, New York, pp. 313-323.

Hogan, B.L., M. Thaller, C. Thaller and G. Eichele. 1992. Evidence that Hensen's node is a source of retinoic acid synthesis. *Nature* 359: 237-241.

Holder N. 1977. An experimental investigation into the early development of the chick elbow joint. J. Embryol. Exp. Morphol. 39: 115-127.

Howlett CR. 1979. The fine structure of the proximal growth plate of the avian tibia. J. Anat. 128: 377-399.

Isogai Z, Aspberg A, Keene DR, Ono RN, Reinhardt DP, Sakai LY. 2002. Versican interacts with fibrillin-1 and links extracellular microfibrils to other connective tissue networks. J. Biol. Chem. 277. 4565-4572.

Ito MM, Kida MY. 2000. Morphological and biochemical re-evaluation of the process of cavitiation in the rat knee joint: cellular and cell strata alterations in the interzone. J. Anat. 197: 659-679.

Johnson R, Tabin C. 1997. Molecular models for vertebrate limb development. Cell 90: 979-90.

Jurand A. 1965. Ultrastructural aspects of early development of the fore-limb buds in the chick and mouse. Proc R Soc Lond (Biol) 162: 387-405.

Kamiya N, and 6 others. 2006. Versican/PG-M regulates chondrogenesis as an extracellular matrix molecule crucial for mesenchymal condensation. J Biol Chem. 281 (4): 2390-400.

Kawakami Y, Capdevila J, Buscher D, Itoh, Rodriguez Esteban C, Izpisua Belmont JC. 2001. WNT signals control FGF-dependent limb initiation and AER induction in the chick embryo. Cell 104: 891-900.

Khan IM, Redman SN, Williams R, Dowthwaite GP, Oldfield SF, Archer CW. 2007. The Development of Synovial Joints. Current Topics in Developmental Biology. 79: 1-36.

Kern CB, and 8 others. 2007. Versican proteolysis mediates myocardial regression during outflow tract development. Dev Dyn. 263(3): 671-683.

Kieny M. 1960. Role inducteur du mesoderme dans la differenciation precoce du ourgeon de member chez l'embryon de poulet. J.Embryol. Exp. Morphol. 8: 457-467.

Kuczuk MH, Scott WJ. 1984. Potentiation of acetazolamide induced ectrodactyly in SwV and C57bL/6J mice by cadmium sulfate. Teratology 29: 427-435.

Le Baron RG, Zimmermann DR, Ruoslahti E. 1992. Hyaluronate binding properties of versican. J. Biol. Chem. 267: 10003-10010.

Lee GM, Johnstone B, Jacobson K, Caterson B. 1993. The dynamic structure of the pericellular matrix on living cells. J Cell Biol. 123: 1899-1907.

Linsenmeyer,T.F., Toole, B.P., and R.L. Trelstad. 1973. Temporal and spatial transitions in collagen types during embryonic chick limb development. Dev. Biol. 35: 232-239.

Lufti AM. 1974. The ultrastructure of cartilage cells in the epiphyses of long bones in the domestic fowl. Acta anatomica 87: 12-21.

MacCabe JA, Errick J, Saunders JW. 1974. Ectodermal control of the dorso-ventral axis in leg bud of chick embryo. Dev. Biol. 39: 69-82.

Mackie EJ, Thesleff I, Chiquet-Ehrisman R. 1987. Tenascin is associated with chondrogenic and osteogenic differentiation in vivo and promotes chondrogenesis in vitro. J. Cell Biol. 105:2569-2579.

Mahmood R, and 9 others. 1995. A role for FGF-8 in the initiation and maintenance of vertebrate limb outgrowth. Curr. Biol. 5: 797-806.

Maleski MP, Knudson CB. 1996. Hyaluronan-Mediated Aggregation of Limb Bud Mesenchyme and Mesenchymal Condensation during Chondrogenesis. Exp. Cell Res. 225: 55-66.

Martin GR. 1998. The roles of FGFs in the early development of vertebrate limbs. Genes Dev. 12: 1571-86.

Marshall H, Morrison A, Studer M, Popperl H, Krumlauf R. 1996. Retinoids and Hox genes. *FASEB J*. 10: 969-78.

Matsumoto K, Shionyu M, Go M, Shimizu K, Shinomura T, Kimata K, Watanabe H. 2003. Distinct interaction of versican/PG-M with hyaluronan and link protein. J Biol Chem. 278:41205-12.

Matsumoto K, Li Y, Jakuba C, Sugiyama Y, Sayo T, Okuno M, Dealy CN, Tool BP, Takeda J, Yamaguchi Y, Kosher RA. 2009. Conditional inactivation of *Has2* reveals a crucial role for hyaluronan in skeletal growth, patterning, chondrocyte maturation and joint formation in the developing limb. *Development*. 136: 2825-2835.

McPherron AC, Lawler AM, Lee SJ. 1999. Regulation of anterior/posterior patterning of the axial skeleton by growth/differentiation factor 11. *Nat Genet*. 22:260-64.

Murray PDF, Selby D. 1930. Extrinsic and intrinsic factors in the primary development of the skeleton. Wilhelm Roux Archiv fur Entwicklungsmechanik der Organismen. 122: 629-662.

Nelson CE, Morgan BA, Burke AC, Laufer E, DiMambro E, et al. 1996. Analysis of Hox gene expression in the chick limb bud. *Development*. 122: 1449-66.

Oberlender SA, Tuan RS. 1994. Expression and functional involvement of N-cadherin in embryonic limb chondrogenesis. Development 120: 177-187.

Ohuchi H, and 11 others. 1997. The mesenchymal factor, FGF10, initiates and maintains the outgrowth of the chick limb bud through interaction with FGF8, and apical ectodermal factor. Development 124: 2235-2244.

Olin AI, Morgelin M, Sasaki T, Timpl R, Heinegard D, Aspberg A. 2001. The proteoglycans aggrecan and versican form networks with fibulin-2 through their lectin domain binding. J. Biol. Chem. 276: 1253-1261.

Oliver G, De Robertis EM, Wolpert L, Tickel C. 1990. Expression of a homeobox gene in the chick wing bud following application of retinoic acid and grafts of polarizing region tissue. EMBO J. 9: 3093-99.

Pacifici M, Iwamoto M, Golden EB, Leatherman JL, Lee YS, Chuong CM. 1993. Tenascin is Associated With Articular Cartilage Development. Dev Dyn 198:123-134.

Pacifici M, Koyama E, Iwamoto M. 2005. Mechanisms of synovial joint and articular cartilage formation: recent advances, but many lingering mysteries. Birth Defects Res. 75: 237-248.

Pfaffl MW. 2001. A new mathematical model for relative quantification in real-time RT-PCR. Nucleic Acids Res. 29: 2002-2007

Pitsillides AA, Archer CW, Prehm P, Bayliss MT, Edwards JCW. 1995. Alterations in hyaluronan synthesis during developing joint cavitation. J Histochem. Cytochem. 43: 263-273.

Rancourt DE, Tsuzuki T, Capecchi MR. 1995. Genetic interaction between hoxb-5 and hoxb-6 is revealed by nonallelic noncomplementation. *Genes Dev*. 9:108-22.

Riddle RD, Johnson RL, Laufer E, Tabin C. 1993. Sonic hedgehog mediates the polarizing activity of the ZPA. Cell 75: 1401-1416.

Rouslahti E. Proteoglycans in cell regulation. J. Biol. Chem. 267: 13369-13372.

Saunders JW. 1948. The proximo-distal sequence of the origin of the parts of the chick wing and the role of the ectoderm. *J. Exp. Zool*. 108, 363-403.

Saunders JW, Gasseling MT. 1968. Ectodermal-mesodermal interactions in the origin of limb symmetry. In R. Fleischmajer and R.E. Billingham (eds.), Epitehlial-Mesenchymal Interactions. Williams &Wilkins, Baltimore, 78-97.

Saunders JW, Reuss C. 1974. Inductive and axial properties of prospective wing-bud mesoderm in the chick embryo. Dev. Biol. 38: 41-50.

Searls RL, Janners MY. 1971. The initiation of limb bud outgrowth in the embryonic chick. *Dev. Biol*. 24: 198-213.

Sekine K, and 10 others. 1999. FGF 10 is essential for limb and lung formation. Nature Genet. 21: 138-141.

Sessions S.K., Gardiner DM, Bryant SV. 1989. Compatible limb patterning mechanisms in urodeles and anurans. *Dev*. *Biol*. 131: 294-301.

Settle SH, Roundtree RB, Sinha A, Thacker A, Higgins K, Kingsley DM. 2003. Multiple joint and skeletal patterning defects caused by single and double mutations in the mouse Gdf5 and Gdf6 genes. Dev. Biol. 254: 116-130.

Sheng W, Wang G, La Pierre DP, Wen J, Deng Z, Wong C-K A, Lee DY, Yang BB. 2006. Versican Mediates Mesenchymal-Epithelial Transition. 17:2009-2020.

Shepard JB, Krug HA, LaFoon BA, Hoffman S, Capehart AA. 2007. Versican Expression during Synovial Joint Morphogenesis. Int. J. Biol. Sci. 3:380-384.

Shi S, Grothe S, Zhang Y, O'Conner-McCourt MD, Poole AR, Roughley PJ, Mort JS. 2004. Link Protein Has Greater Affinity for Versican than Aggrecan. J. Biol. Chem. 279: 12060-12066.

Shinomura, T., Nishida, Y., Ito, K., and Kimata, K. 1993. cDNA cloning of PG-M, a large chondroitin sulfate proteoglycan expressed during chondrogenesis in chick limb buds. Alternative spliced multiforms of PG-M and their relationships to versican. J. Biol. Chem. 268, 14461-14469.

Storm EE, Huynh TV, Copeland NG, Jenkins NA, Kingsley DM, Lee S. 1994. Limb alterations in brachypodism mice due to mutations in a new member of the TGFß-superfamily. Nature 368: 639-643.

Storm EE, Kingsley DM. 1996. Joint patterning defects caused by single and double mutations in members of the bone morphogenetic protein (BMP) family. Development 122: 3969-79.

Stratford,T., C. Horton and M. Maden. 1996. Retinoic acid is required for the initiation of outgrowth in the chick limb bud. *Curr Biol*. 6: 1124-1133.

Summerbell D, Lewis JH, Wolpert L. 1973. Positional information in chick limb morphogenesis. Nature 244: 492-96.

Suwan K, Choocheep K, Hatano S, Kongtawelert P, Kimata K, Watanabe H. 2009. Versican/PG-M Assembles Hyaluronan into Extracellular Matrix and Inhibits CD44-mediated Signaling toward Premature Senescence in Embryonic Fibroblasts. J Biol Chem 284: 8596-604.

Thorogood P, Hinchliffe J. 1975. An analysis of the condensation process during chondrogenesis in the embryonic chick hind limb. J Embryol Exp Morphol 33: 581-606.

Tickel C, Summerbell D, Wolpert L. 1975. Positional signaling and specification of digits in chick limb morphogenesis. Nature 254: 199-202.

Tickel C, Altabef M. 1999. Epithelial cell movement and interactions in limb, neural crest, and vasculature. Curr Opin Genet Dev. 9(4): 455-60

Vogel A, Rodriguez C, Izpisua-Belmont JC. 1996. Involvement of FGF-8 in initiation, outgrowth, and patterning of the vertebrate limb. Development 122: 1737-1750.

Watanabe H., Yamada Y. 2003. Chondroplasia of gene knockout mice for aggrecan and link protein. Glycoconjugate Journal 19, 269-273.

Wight TN. 2002. Versican: a versatile extracellular matrix proteoglycan in cell biology. Curr Opin Cell Biol. 14: 617-23.

Williams DR, Presar AR, Richmond AT, Mjaatvedt CH, Hoffman S, Capehart AA. 2005. Limb chondrogenesis is compromised in the versican deficient hdf mouse. Biochem. Biophys. Res. Comm. 334: 960-966.

Yamagata M, Yamada KM, Yoneda M, Suzuki S, Kimata K. 1986. Chondrotin sulfate proteoglycan (PG-M-like proteoglycan) is involved in the binding of hyaluronic acid to cellular fibronectin. J Biol Chem 15: 13526-13535.

Yamagata M, Suzuki S, Akiyama SK, Yamada KM, Kimata K. 1989. Regulation of cell-substrate adhesion by proteoglycans immobilized on extracellular substrates. J Biol. Chem. 264: 8012-8018.

Yamagata M, Shinomura T, Kimata K. 1993. Tissue variation of two large chondroitin sulfate proteoglycans (PG-M/versican and PG-H/aggrecan) in chick embryos. Anat Embryol. 187: 433-44.

Yamagata M, Kimata K. 1994. Repression of a malignant cell-substratum adhesion phenotype by inhibiting the production of the anti-adhesive proteoglycan, PG-M/versican. J.Cell Sci 107: 2581-90.

Zanin MKB, Bundy J, Ernst H, Wessels A, Conway SJ, Hoffman S. 1999. Distinct spatial and temporal distributions of aggrecan and versican in the embryonic chick heart. Anat Rec. 256: 366-80.

Zimmerman DR, Rouslahti E. 1989. Multiple domains of the large fibroblast proteoglycan, versican. Embo J. 8(10): 2975-2981.

Appendix A: Animal Use Protocol

Animal Care and Use Committee
East Carolina University
212 Ed Warren Life Sciences Building
Greenville, NC 27834
252-744-2436 office • 252-744-2355 fax

March 27, 2009

Anthony Capehart, Ph.D.
Department of Biology
C407 Howell Science Complex
East Carolina University

Dear Dr. Capehart:

Your Animal Use Protocol entitled, "Effect of Versican Mutation on Limb Development In Vitro," (AUP #D207a) was reviewed by this institution's Animal Care and Use Committee on 3/27/09. The following action was taken by the Committee:

"Approved as submitted"

A copy is enclosed for your laboratory files. Please be reminded that all animal procedures must be conducted as described in the approved Animal Use Protocol. Modifications of these procedures cannot be performed without prior approval of the ACUC. The Animal Welfare Act and Public Health Service Guidelines require the ACUC to suspend activities not in accordance with approved procedures and report such activities to the responsible University Official (Vice Chancellor for Health Sciences or Vice Chancellor for Academic Affairs) and appropriate federal Agencies.

Sincerely yours,

Robert G. Carroll, Ph.D.
Chairman, Animal Care and Use Committee

RGC/jd

enclosure

Appendix B: Permission Letter

Dear Mr. partha nagchowdhuri,

Thank you for placing your order through Copyright Clearance Center's RightsLink service. John Wiley and Sons has partnered with RightsLink to license its content. This notice is a confirmation that your order was successful. Your order details and publisher terms and conditions are available by clicking the link
below: http://s100.copyright.com/CustomerAdmin/PLF.jsp?lID=2012091_1348770670004

Order Details Licensee: partha s nagchowdhuri License Date: Sep 27, 2012

License Number: 2997200430004 Publication: The Anatomical Record:

Advances in Integrative Anatomy and Evolutionary Biology Title: Versican

Knockdown Reduces Interzone Area During Early Stages of Chick Synovial Joint

Development Type Of Use: Dissertation/Thesis Total: 0.00 USD

Appendix C: PhosphoHistone Assay

Figure C1. Phosphohistone antibody staining of paraffin sections through HH stage 36 elbows, 5 days following injection with 5334 (**A-D**) and control sh-RNA adenoviruses (**E-H**). Boxed area in panel **B** indicates fewer histone positive cells than in the boxed area in the CLC wing (**A**). This difference in the number of histone-positive cells between the injected and CLC wings is not apparent in the embryo injected with the control sh-RNA adenovirus. There seems to be almost the same number of histone positive cells in both the injected joint interzone (**F**) as well as the CLC interzone (**E**). Panels **G** and **H** are phase contrast and bright images respectively of the CLC wing and the injected wing. Panel **H** shows thorough transfection of the control sh-RNA in the humero-ulnar interzone. Scale bar= 50μm (C). Scale bar for all other panels = 100μm.

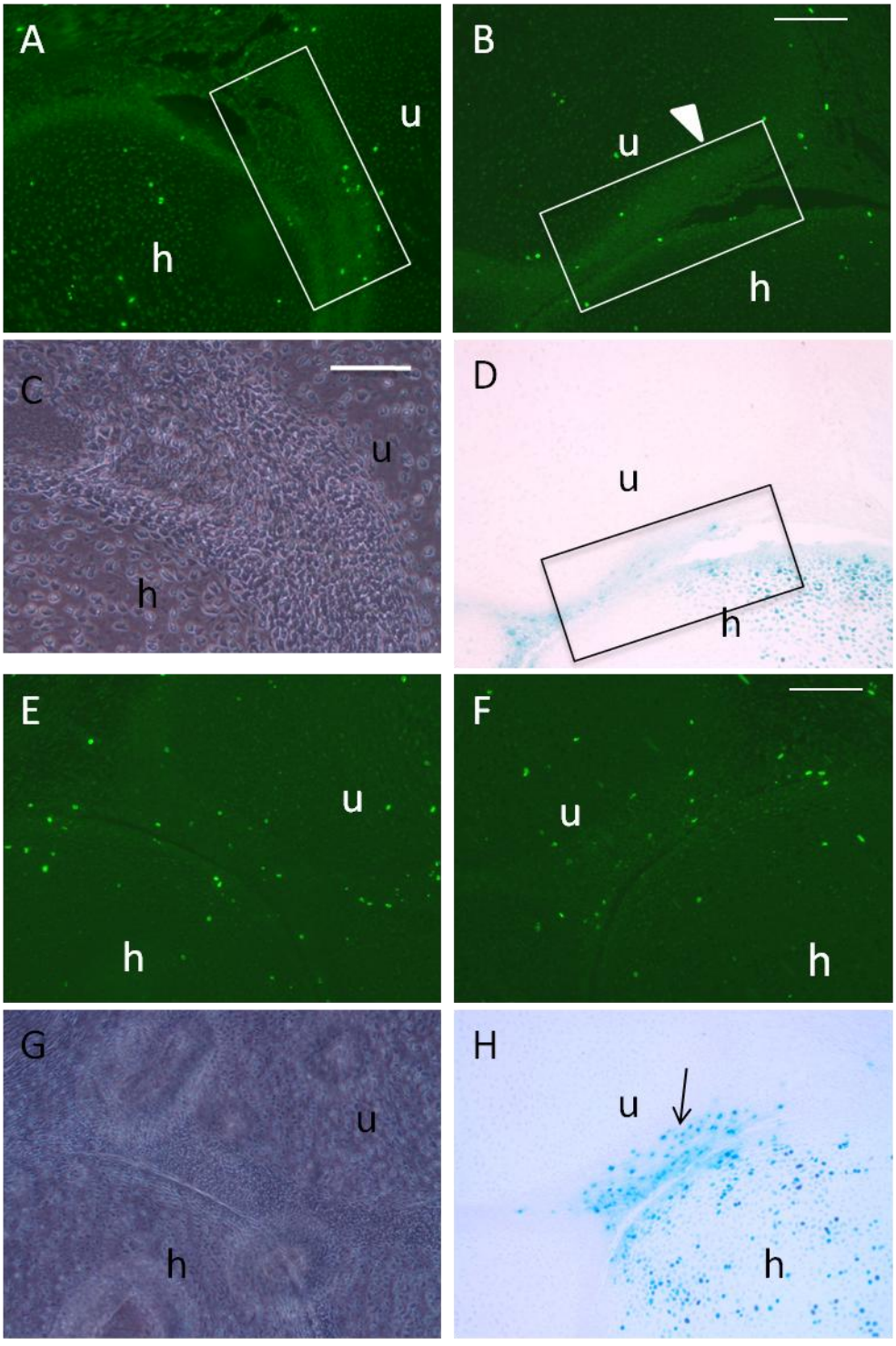
A
u
h
B
u
h
C
u
h
D
u
h
E
u
h
F
u
h
G
u
h
H
u
h

Appendix D: Cell Size Measurements

Figure D1. Bar Graph representing alterations in the size of joint interzone cells (in square-micrometers) as a result of matrix vesican knockdown. A significant (~24%) reduction in area was observed for joint interzone cells infected with the experimental shRNAs (320, 5334, and 320+5334 combined shRNAs) adenoviruses when compared to interzone cells of the CLC wing. No significant difference in interzone cell area was noted for wings injected with the control shRNA when compared with the CLC wing. The slight difference in average cell area between the injected and CLC wings is possibly due to precipitates forming on cell surface resulting from the reaction between X-gal and ß-galactosidase.